

CP violations in a predictive A_4 symmetry model

T. Phong Nguyen,^{1,*} L. T. Hue,^{2,†} D. T. Si,^{2,‡} and T. T. Thuc^{3,§}

¹*Department of Physics, Can Tho University, 3/2 Street, Can Tho, Vietnam*

²*Institute of Research and Development,*

Duy Tan University, Da Nang 550000, Vietnam

³*Department of Education and Training of Ca Mau, 70 Phan Dinh Phung, Vietnam*

Abstract

We will investigate numerically a seesaw model with A_4 flavor symmetry to find allowed regions satisfying the current experimental neutrino oscillation data, then use them to predict physical consequences. Namely, the lightest active neutrino mass is of the order of $\mathcal{O}(10^{-2})$ eV. The effective neutrino mass $|\langle m \rangle|$ associated with neutrinoless double beta decay is in the range $[0.002 \text{ eV}, 0.038 \text{ eV}]$ and $[0.048 \text{ eV}, 0.058 \text{ eV}]$, corresponding to the normal and the inverted hierarchy schemes, respectively. Other relations among relevant physical quantities are shown, so that they can be determined if some of them are confirmed experimentally. The recent data of the baryon asymmetry of the Universe (η_B) can be explained via leptogenesis caused by the effect of the renormalization group evolution on the Dirac Yukawa couplings, provided the right-handed neutrino mass scale M_0 ranges from $\mathcal{O}(10^8)$ GeV to $\mathcal{O}(10^{12})$ GeV for $\tan \beta = 3$. This allowed M_0 range is different from the scale of $\mathcal{O}(10^{13})$ GeV for other effects that also generate a consistent η_B from leptogenesis. The branching ratio of the decay $\mu \rightarrow e\gamma$ may reach future experimental sensitivity for very light values of M_0 . Hence, it will be inconsistent with the M_0 range predicted from the η_B data whenever this decay is detected experimentally.

PACS numbers:

*Electronic address: thanhphong@ctu.edu.vn

†Electronic address: lethohue@duytan.edu.vn

‡Electronic address: dangtrungsi@duytan.edu.vn

§Electronic address: truongtrongthuck17@gmail.com

I. INTRODUCTION

The experimental data for neutrino oscillation definitely affirmed that neutrinos are massive and they are mixing. Based on neutrino experimental data, in 2002, P. F. Harrison et al. [1–4] proposed the structure of neutrino mixing matrix named tri-bimaximal (TB). According to this structure, the reactor mixing angle, θ_{13} , is zero and the Dirac CP-violating phase has no meaning. Subsequently, there was a lot of effort to build simple models leading to the TB mixing pattern of leptons. An interesting way seems to be the use of some discrete non-Abelian flavor groups added to the gauge group of the Standard Model (SM). There is a series of such models based on the symmetry groups A_4 [5–11], T' [12–15], and S_4 [16–19]. These models are usually realized at some high-energy scale Λ and the groups are spontaneously broken due to a set of scalar multiplets. On the other hand, the most up-to-date data from neutrino oscillation experiments shows that the reactor mixing angle is relatively large, $\theta_{13} \sim 8^\circ$ [20]. As a result, the models mentioned have been improved in order to generate a non-zero value of θ_{13} as well as leptogenesis; see, for example the models with A_4 symmetry given in Refs. [8, 21–24], where higher-order corrections to fermion mass matrices were considered. However, according to these works, just the inclusion of higher-order corrections would not produce such a large value of θ_{13} consistent with experiment. Improved models with modular A_4 symmetry groups have also been constructed recently to explain the neutrino oscillation data [25, 26]. On the other side, several models were built by adding new sources of A_4 breaking at the leading orders into the original A_4 models [8], so that they can successfully explain both experimental values of θ_{13} and leptogenesis; see, for example, Refs. [11, 24, 27–29], and a list of other models reviewed in Ref. [30]. In particular, a soft breaking A_4 term was introduced in Ref. [11], three singlet flavons were used in Refs. [24, 27], and two singlet flavons ξ, ξ' transform as $1, 1'$ of the A_4 in Refs. [24, 28, 29] in order to accommodate with the present neutrino data. However, leptogenesis was not studied in Ref. [28], while in Ref. [29], to explain conventional leptogenesis the authors considered the contribution of the next-to-leading order (NLO) corrections to the right-handed neutrino (RHN) mass matrix in the supersymmetry framework. Namely, two new NLO terms corresponding to two new independent parameters were introduced by hand, then their allowed values were investigated to guarantee successful leptogenesis, leading to a prediction that the RHN mass scale is around $\mathcal{O}(10^{13})$ GeV. But these terms will not survive

in other models where new charge assignments of discrete symmetries are chosen to cancel them. In addition, it seems that this approach still needs more independent parameters than an alternative presented in Ref. [11], where a single softly broken A_4 term was added into the original model to successfully solve both neutrino data and leptogenesis, leading to a prediction of the RHN mass scale of $O(10^{13})$ GeV. The model mentioned in Ref. [11] is the simplest extension of the original one discussed in Ref. [8].

In this work we will study another simple approach, based on the model introduced in Ref. [29], but only effects of renormalization group (RG) evolution of the Dirac Yukawa coupling matrix will be included to study flavored leptogenesis. Because only two flavon singlets are added into the model, and the NLO terms like those mentioned in Ref. [29] are excluded by the total symmetry, only one new term appears in the model, therefore it is also as simple as the model given in Ref. [11]. We believe that the effect caused by just the RG is as important as the effects arising from the NLO terms mentioned in Ref. [29], where successful leptogenesis requires a large RHN mass scale of around $O(10^{13})$ GeV. Also, the same RHN mass scale is needed for successful leptogenesis in the model constructed in Ref. [11]. This scale is only three orders less than the perturbative limit of the seesaw (SS) model [31–35] $\sqrt{4\pi} \times 174/10^{-12} \sim O(10^{16})$. Our work will find an interesting answer for the question of whether the RG effects need a lower RHN mass scale to explain leptogenesis, or whether they have the same order of 10^{13} GeV predicted previously. Anyway, we can discuss which effects are dominant or whether there any properties to distinguish these two effects if they appear simultaneously in the same RHN mass scale. The correlation of the two effects will also be very interesting, but we will leave this for further study.

Besides generating a tiny neutrino mass, the seesaw model has another physics consequence called leptogenesis for the generation of the observed baryon asymmetry of the Universe (BAU) by the charge/parity (CP) asymmetric decay of heavy RHNs [36–38]. If the BAU was generated by leptogenesis, then CP-violation in the lepton sector must exist. For Majorana neutrinos, there are one Dirac and two Majorana CP violating phases. One of the phases (or a combination of them) in principle can be measured by neutrinoless double beta ($0\nu 2\beta$) decay [39–42] experiments. Also, the TB mixing structure forbids low-energy CP violation in neutrino oscillation, due to $U_{e3} = 0$, and also forbids high-energy CP violation in leptogenesis. Therefore, any observations of leptonic CP violation, for instance in $0\nu 2\beta$ decay, can strengthen our believe in leptogenesis by demonstrating that CP is not a

lepton symmetry.

In this work we consider an expansion of the SM by the seesaw realization of an A_4 discrete symmetric model and its phenomena. Apart from two SM scalar doublets taking responsibility for spontaneously breaking of A_4 and the SM gauge groups, this model contains additional $SU(2)_L$ scalar singlets, namely two singlets ξ', ξ'' transform as $1', 1''$ and two triplets of the A_4 . If the RHN mass matrix's components resulting from the contributions of the vacuum expectation values (VEVs) of two scalar singlets (of both $SU(2)_L$ and A_4) are exactly the same, then the model generates the TB pattern of lepton mixing matrix and hence leptogenesis does not work. We therefore study the case where those components are independent, and we find the allowed regions of the parameter space of the model that satisfy the low-energy data and the recent BAU data through flavored leptogenesis that arise from the RG effects at a high scale of RHN masses. At low-energy, although our model inherits similar properties in the lepton sector to some previous works [29], where some of the unknown parameters were fixed to determine the allowed regions, in this work we will scan the whole parameter space to collect all possible allowed regions satisfying the recent neutrino oscillation data. Based on this, we give interesting physical consequences of $|\langle m \rangle|$ and lepton flavor violating (LFV) decays. We will also determine the RHN mass scale at high energy that successfully explains the BAU data originating from just the RG effect. The allowed range of RHN mass scale will be used to compare with those concerned previously, which come from other sources of soft breaking A_4 or NLO terms that are forbidden in our model.

This work is organized as follows. In Sect. II we summarize all the ingredients for constructing the A_4 model with the seesaw mechanism, focusing on the Higgs and lepton sectors. After that, we present, step by step, our approach to numerically investigating the parameter space of the model to guarantee that all allowed regions satisfying the recent neutrino oscillation data are pointed out. Following this, we continue predicting some consequences related to the low-energy phenomena of the lepton sector. Section III is devoted to studying the leptogenesis originating purely from the RG effects, where the allowed range of the RHN mass scale that satisfies the BAU data will be determined. Section IV will pay attention to the LFV decay of charged leptons, and will show that these decays can be considered as another indirect channel to estimate the RHN mass scale. Important conclusions from our work are given in the last section, section V. In addition, there are three appendices to

add more detailed discussions on the A_4 rules, the Higgs potential, and analytic formulas for one-loop contributions to the LFV decays in the unitary gauge.

II. THE A_4 SYMMETRY MODEL WITH SEESAW MECHANISM

The non-Abelian A_4 is a group of even permutations of four objects and has $4!/2 = 12$ elements. All the properties of this group needed for model construction were given in Ref. [8]. This paper will work in the A_4 basis introduced by G. Altarelli and F. Feruglio, as reviewed in Appendix A. In this work we promote the A_4 proposed in Refs. [11, 29] with two Higgs singlets to accompany the seesaw mechanism. The model contains several $SU(2)_L \otimes U(1)_Y$ Higgs singlets, where two of them (ξ' , ξ'') are A_4 singlets, while the remaining (ϕ_S , ϕ_T) are triplets. The SM lepton doublets are assigned to be three components of one A_4 triplet, while three right-handed charged leptons e_R, μ_R, τ_R are assumed to transform as three different singlets $1, 1'', 1'$, respectively. The standard Higgs doublets h_u and h_d remain invariant under A_4 . The particle content for leptons and scalars, their VEVs, and the symmetry groups considered in the model are shown in Table I. Two more discrete symmetries, Z_3 and Z_4 , are included in order to get minimal and necessary Yukawa couplings.

The Lagrangian for the lepton sector which is invariant under all the symmetries given in Table I is

$$\begin{aligned}
-\mathcal{L} = & \frac{y_e}{\Lambda}(\phi_T \bar{\psi}_L^l) e_R h_d + \frac{y_\mu}{\Lambda}(\phi_T \bar{\psi}_L^l)'' \mu_R h_d + \frac{y_\tau}{\Lambda}(\phi_T \bar{\psi}_L^l)' \tau_R h_d + p \bar{\psi}_L^l N_R h_u \\
& + x_A' \xi' (\bar{N}_L^c N_R)'' + x_A'' \xi'' (\bar{N}_L^c N_R)' + x_B (\phi_S \bar{N}_L^c N_R) + \text{H.c.},
\end{aligned} \tag{1}$$

where $N_L^c \equiv C(\bar{N}_R)^T$ and Λ is the cut-off scale of the model. It can be seen that the NLO term like $(\bar{\psi}_L^l N_R \phi_T h_u / \Lambda)$ mentioned in Ref. [29] does not respect the Z_4 symmetry, hence this term vanishes in our model. After spontaneous symmetry breaking, the charged lepton mass matrix comes out diagonally with $m_e = \frac{y_e v_T v_d}{\Lambda}$, $m_\mu = \frac{y_\mu v_T v_d}{\Lambda}$, and $m_\tau = \frac{y_\tau v_T v_d}{\Lambda}$. The couplings y_e, y_μ , and y_τ are naturally the same order of magnitude. In order to produce the mass hierarchy of charged leptons, we make use of an additional spontaneously broken $U(1)_{FN}$ flavor [43]. We introduce a singlet θ carrying $U(1)_{FN}$ charge -1 and neutral under all other symmetries. Its VEV, $\langle \theta \rangle / \Lambda < 1$, breaks $U(1)_{FN}$ and provides expansion parameters for charged lepton masses. We also assign $U(1)_{FN}$ charges $(2n, n)$ to fields (e_R, μ_R) . All other lepton fields are assigned to be neutral under this symmetry. In this way, $y_\tau : y_\mu :$

TABLE I: List of fermion and scalar fields, where $\overline{\psi^l} = (\overline{\nu_{La}}, \overline{e_{La}})^T$ ($a = 1, 2, 3$) and $\omega = e^{2i\pi/3}$.

Lepton	$SU(2)_L$	$U(1)_Y$	A_4	Z_3	Z_4	
$\overline{\psi^l}$	2^*	1	$\underline{3}^*$	1	1	
e_R	1	-2	$\underline{1}$	1	-1	
μ_R	1	-2	$\underline{1}'$	1	-1	
τ_R	1	-2	$\underline{1}''$	1	-1	
N_R	1	0	$\underline{3}$	ω	$-i$	
Scalar	VEV					
h_u	2	-1	$\underline{1}$	ω^2	i	$\langle h_u \rangle = v_u$
h_d	2	1	$\underline{1}$	1	1	$\langle h_d \rangle = v_d$
ϕ_S	1	0	$\underline{3}$	ω	-1	$\langle \phi_S \rangle = (v_S, v_S, v_S)$
ϕ_T	1	0	$\underline{3}$	1	-1	$\langle \phi_T \rangle = (v_T, 0, 0)$
ξ'	1	0	$\underline{1}'$	ω	-1	$\langle \xi' \rangle = u'$
ξ''	1	0	$\underline{1}''$	ω	-1	$\langle \xi'' \rangle = u''$

$y_e = 1 : (\langle \theta \rangle / \Lambda)^n : (\langle \theta \rangle / \Lambda)^{2n}$, and the charged lepton mass hierarchy can be produced by choosing $(\langle \theta \rangle / \Lambda)^n \simeq \lambda^2$, where $\lambda \simeq 0.225$ is the Wolfenstein parameter.

Regarding the quark sector, under the symmetry $SU(3)_C \otimes SU(2)_L \otimes U(1)_Y \otimes A_4 \otimes Z_3 \otimes Z_4$, they can be assigned as follows: $Q_{iL} = (u_i, d_i)_L^T \sim (3, 2, 1/3, \underline{1}, 1, 1)$, $u_{iR} \sim (3, 1, 4/3, \underline{1}, w, -i)$, and $d_{iR} \sim (3, 1, -2/3, \underline{1}, w^2, i)$. Accordingly, the Yukawa Lagrangian of the quarks has the same form as given in the SM, namely

$$\mathcal{L}_q^Y = -Y_{ij}^u \overline{Q_{iL}} h_u u_{jR} - Y_{ij}^d \overline{Q_{iL}} \tilde{h}_u d_{jR} + \text{h.c.}, \quad (2)$$

where $\tilde{h}_u = i\sigma_2 h_u^*$. Although the phenomenology of the quark will not be considered in this work, the Yukawa couplings of the top quark with h_u given in Eq. (2) will give a top quark mass $m_t \simeq Y_{33}^q v_u$, which requires large v_u to generate the well-known top quark mass while Y_{33}^q satisfies the perturbative limit. This also implies a large v_u/v_d , which will be chosen for numerical investigation.

Before continuing to the lepton sector, we note that the VEV structure of the scalar fields assumed in Table I are realistic; see a detailed discussion on the Higgs potential in Appendix B. We have also shown that the model contains an SM-like Higgs boson found

experimentally by LHC [44, 45].

For the charged Higgs boson, in the basis $(H_u^\pm, H_d^\pm)^T$ the squared mass matrix is

$$M_{\text{charged}}^2 = \lambda_4 \times \begin{pmatrix} v_d^2 & v_d v_u \\ v_d v_u & v_u^2 \end{pmatrix}. \quad (3)$$

It gives two pairs of mass eigenstate denoted as physical Higgs bosons φ^\pm and massless states G^\pm which are Goldstone bosons eaten by gauge bosons W^\pm . The masses and relations between the original and mass base of the charged Higg components are as follows,

$$\begin{aligned} m_{G^\pm}^2 &= 0, & G^\pm &= s_\beta H_u^\pm - c_\beta H_d^\pm, \\ m_{\varphi^\pm}^2 &= \lambda_4 v^2, & \varphi^\pm &= c_\beta H_u^\pm + s_\beta H_d^\pm, \end{aligned} \quad (4)$$

where $s_\beta \equiv \sin \beta$, $c_\beta \equiv \cos \beta$, and β is a mixing angle defined by

$$t_\beta \equiv \tan \beta = \frac{v_u}{v_d}, \quad (5)$$

which is similar to the case of the ratio defined by the two VEVs in the minimal supersymmetric Standard Model (MSSM). The charged Higgs boson and the parameter β play very important roles for generating leptogenesis in our model. We emphasize that these two ingredients are independent from all Higgs self couplings of the $SU(2)_L$ Higgs singlets.

To identify the gauge bosons with those in the SM, we start from the covariant derivative for local $SU(2)_L \otimes U(1)_Y$ symmetry. It is defined as

$$D_\mu = \partial_\mu - ig T^a W_\mu^a - i \frac{g'}{2} B_\mu Y, \quad (6)$$

which is the same as in the SM. Here, T^a ($a = 1, 2, 3$) are the generators of the $SU(2)_L$ symmetry. $T^a = \frac{\sigma^a}{2}$ for doublets, and $T^a = 0$ for singlets.

The kinetic terms of all Higgses are

$$\begin{aligned} \mathcal{L}_{\text{kin}}^H &= (D_\mu h_u)^\dagger (D^\mu h_u) + (D_\mu h_d)^\dagger (D^\mu h_d) \\ &+ [(\partial_\mu \phi_T)^\dagger \partial^\mu \phi_T]_{\underline{1}} + [(\partial_\mu \phi_S)^\dagger \partial^\mu \phi_S]_{\underline{1}} + \partial_\mu \xi' \partial^\mu \xi' + \partial_\mu \xi'' \partial^\mu \xi''. \end{aligned} \quad (7)$$

From Table I, where all neutral Higgs singlets have zero $U(1)_Y$ charges, we can see that all $SU(2)_L$ singlets do not couple with gauge bosons. The mass term of the gauge bosons is

$$\mathcal{L}_m^{\text{gauge}} = \frac{g^2(v_u^2 + v_d^2)}{2} W^{+\mu} W_\mu^- + \frac{g^2(v_u^2 + v_d^2)}{4} (W_3 - t_W B)^\mu (W_3 - t_W B)_\mu, \quad (8)$$

where $W^\pm \equiv (W^1 \mp iW^2)/\sqrt{2}$ and $t_W \equiv g'/g$. Matching with the mass of the SM gauge boson W^\pm we obtain the same relation shown in two Higgs doublet models (2HDMs),

$$v^2 = v_u^2 + v_d^2 = 174^2 \text{GeV}^2, \quad t_W = \frac{s_W}{c_W}, \quad (9)$$

where $s_W^2 = 0.231$. It is easy to show that the second term in Eq. (8) implies the presence of the photon and neutral Z boson defined in the SM.

Regarding the lepton, the neutrino sector gives rise to the following Dirac and Majorana neutrino mass matrices:

$$m_D = pv_u \begin{pmatrix} 1 & 0 & 0 \\ 0 & 1 & 0 \\ 0 & 0 & 1 \end{pmatrix} = v_u Y_\nu, \quad Y_\nu = p \times \mathbf{1}, \quad (10)$$

$$M_R = \begin{pmatrix} \frac{2X}{3} & \tilde{Z} - \frac{X}{3} & \tilde{Y} - \frac{X}{3} \\ \tilde{Z} - \frac{X}{3} & \tilde{Y} + \frac{2X}{3} & -\frac{X}{3} \\ \tilde{Y} - \frac{X}{3} & -\frac{X}{3} & \tilde{Z} + \frac{2X}{3} \end{pmatrix} = M_0 \begin{pmatrix} 1 & \tilde{\kappa} - \frac{1}{2} & \tilde{\rho} - \frac{1}{2} \\ \tilde{\kappa} - \frac{1}{2} & \tilde{\rho} + 1 & -\frac{1}{2} \\ \tilde{\rho} - \frac{1}{2} & -\frac{1}{2} & \tilde{\kappa} + 1 \end{pmatrix}, \quad (11)$$

where $X = 2x_B v_S$, $\tilde{Y} = 2x'_A u'$, $\tilde{Z} = 2x''_A u''$, and $M_0 = 2X/3$ is the scale of the RHN mass, $\tilde{\kappa} = \tilde{Z}/M_0$, $\tilde{\rho} = \tilde{Y}/M_0$. We assume that M_0 is real and positive. Hereafter, complex parameters are distinguished by tildes. Then, the active neutrino mass matrix is then obtained by the seesaw formula [31–35]:

$$m_\nu = -v_u^2 Y_\nu^T M_R^{-1} Y_\nu. \quad (12)$$

This matrix is used to determine the active neutrino masses $m_{1,2,3}$ and neutrino mixing matrix U_ν , namely

$$U_\nu^T m_\nu U_\nu = \text{diag}(m_1, m_2, m_3) \equiv m_\nu^d, \quad (13)$$

where $m_{1,2,3}$ is positive real, and the lepton mixing matrix $U_{\text{PMNS}} = U_\nu$ since the charged lepton mass matrix is diagonal in our case. For later convenience, at first we diagonalize the right-handed neutrino mass matrix M_R based on the nearly TB forms discussed previously. In particular, if $\tilde{\rho} = \tilde{\kappa}$ then M_R is exactly diagonalized by the well-known TB structured matrix, namely

$$U_{\text{TB}} = \begin{pmatrix} \sqrt{\frac{2}{3}} & \frac{1}{\sqrt{3}} & 0 \\ -\frac{1}{\sqrt{6}} & \frac{1}{\sqrt{3}} & -\frac{1}{\sqrt{2}} \\ -\frac{1}{\sqrt{6}} & \frac{1}{\sqrt{3}} & \frac{1}{\sqrt{2}} \end{pmatrix}. \quad (14)$$

Hence, the non-zero s_{13} may arise from the deviation of these two parameters. Furthermore, s_{13} is found experimentally to be rather smaller than 1, which suggests that the deviation should be small. Hence, in this work we adopt that $\tilde{\rho} = \tilde{\kappa}(1 + \epsilon)$, where ϵ is a complex parameter satisfying $|\epsilon| < 1$, so that it will be used as a reliable perturbative parameter in the next approximate calculations. Then the matrix M_R is rewritten in a new form as

$$M_R = M_0 \begin{pmatrix} 1 & \tilde{\kappa} - \frac{1}{2} & \tilde{\kappa}(1 + \epsilon) - \frac{1}{2} \\ \tilde{\kappa} - \frac{1}{2} & \tilde{\kappa}(1 + \epsilon) + 1 & -\frac{1}{2} \\ \tilde{\kappa}(1 + \epsilon) - \frac{1}{2} & -\frac{1}{2} & \tilde{\kappa} + 1 \end{pmatrix}. \quad (15)$$

This matrix is diagonalized by a unitary matrix U_R defined as follows

$$M_R^d = U_R^T M_R U_R = \text{diag}(M_1, M_2, M_3), \quad (16)$$

where

$$\begin{aligned} M_1 &= M_0 \left| \frac{1}{2}(3 - 2\sqrt{\tilde{\kappa}^2 \epsilon^2 + \tilde{\kappa}^2 \epsilon + \tilde{\kappa}^2}) \right| = M_0 \left| \frac{1}{2}(3 - 2\tilde{\kappa}\sqrt{1 + \epsilon + \epsilon^2}) \right|, \\ M_2 &= M_0 |\tilde{\kappa}(2 + \epsilon)|, \\ M_3 &= M_0 \left| \frac{1}{2}(3 + 2\sqrt{\tilde{\kappa}^2 \epsilon^2 + \tilde{\kappa}^2 \epsilon + \tilde{\kappa}^2}) \right| = M_0 \left| \frac{1}{2}(3 + 2\tilde{\kappa}\sqrt{1 + \epsilon + \epsilon^2}) \right| \end{aligned} \quad (17)$$

are masses of physical RHNs, and the matrix U_R is determined through two steps, where the first relates to U_{TB} , while the second is a product of a unitary matrix U_1 depending on ϵ and a phase matrix U_P . The precise form is

$$U_R = U_{\text{TB}} U_1 U_P, \quad U_1 = \begin{pmatrix} c_\theta & 0 & s_\theta e^{i\zeta} \\ 0 & 1 & 0 \\ -s_\theta e^{-i\zeta} & 0 & c_\theta \end{pmatrix}, \quad U_P = \begin{pmatrix} e^{-i\varphi_1/2} & 0 & 0 \\ 0 & e^{-i\varphi_2/2} & 0 \\ 0 & 0 & e^{-i\varphi_3/2} \end{pmatrix}, \quad (18)$$

$$\begin{aligned} \varphi_1 &= \arg(3 - 2\tilde{\kappa}\sqrt{1 + \epsilon + \epsilon^2}), \quad \varphi_2 = \arg \tilde{\kappa}(2 + \epsilon) = \phi, \\ \varphi_3 &= \arg(3 + 2\tilde{\kappa}\sqrt{1 + \epsilon + \epsilon^2}), \end{aligned} \quad (19)$$

where s_θ is positive and ζ is real. We note that the consideration that $M_{1,2,3}$ are physical RHNs is consistent in the seesaw limit, as we will point out later.

Because of the diagonal form of the matrix Y in the light neutrino mass matrix m_ν given in Eq. (12), it is diagonalized exactly using U_R through the following intermediate transformation:

$$m_\nu = v_u^2 Y_\nu^T \left(U_R^* M_R^d U_R^\dagger \right)^{-1} Y_\nu$$

$$= U_R \text{diag}(m_1, m_2, m_3) U_R^T \equiv U_\nu^* m_\nu^d U_\nu^\dagger, \quad (20)$$

where m_ν^d was defined previously in Eq. (13), and the active neutrino masses are formulated as follows:

$$\begin{aligned} m_1 &= \frac{(v_u p)^2}{M_1} = \frac{2m_0}{|3 - 2\tilde{\kappa}\sqrt{1 + \epsilon + \epsilon^2}|} = \frac{2m_0}{\sqrt{(3 - 2\kappa\sqrt{1 + \epsilon + \epsilon^2}c_\phi)^2 + (2\kappa\sqrt{1 + \epsilon + \epsilon^2}s_\phi)^2}} \\ m_2 &= \frac{(v_u p)^2}{M_2} = \frac{m_0}{|(2 + \epsilon)\tilde{\kappa}|} = \frac{m_0}{(2 + \epsilon)\kappa}, \\ m_3 &= \frac{(v_u p)^2}{M_3} = \frac{2m_0}{|3 + 2\tilde{\kappa}\sqrt{1 + \epsilon + \epsilon^2}|} = \frac{2m_0}{\sqrt{(3 + 2\kappa\sqrt{1 + \epsilon + \epsilon^2}c_\phi)^2 + (2\kappa\sqrt{1 + \epsilon + \epsilon^2}s_\phi)^2}}, \end{aligned} \quad (21)$$

where

$$m_0 = \frac{(v_u p)^2}{M_0} \quad (22)$$

is real and positive.

As we can see, since the charged lepton matrix is diagonal, the lepton mixing matrix U_{PMNS} is, apart from the diagonal Majorana CP-violating phase matrix U'_P , exactly the neutrino mixing matrix U_ν , namely

$$U_{\text{PMNS}} \equiv U_\nu = U_R^* = U_{\text{TB}} U_1^* U_P^* \quad (23)$$

$$= e^{i\varphi_1} \begin{pmatrix} \sqrt{\frac{2}{3}}c_\theta & \sqrt{\frac{1}{3}} & \sqrt{\frac{2}{3}}s_\theta e^{-i\zeta} \\ \frac{-c_\theta}{\sqrt{6}} + \frac{s_\theta}{\sqrt{2}}e^{i\zeta} & \sqrt{\frac{1}{3}} & \frac{-c_\theta}{\sqrt{2}} - \frac{s_\theta}{\sqrt{6}}e^{-i\zeta} \\ \frac{-c_\theta}{\sqrt{6}} - \frac{s_\theta}{\sqrt{2}}e^{i\zeta} & \sqrt{\frac{1}{3}} & \frac{c_\theta}{\sqrt{2}} - \frac{s_\theta}{\sqrt{6}}e^{-i\zeta} \end{pmatrix} \begin{pmatrix} 1 & 0 & 0 \\ 0 & e^{i(\varphi_2 - \varphi_1)/2} & 0 \\ 0 & 0 & e^{i(\varphi_3 - \varphi_1)/2} \end{pmatrix} \quad (24)$$

Comparing with the standard parametrization of U_{PMNS} [20],

$$U_{\text{PMNS}} = \begin{pmatrix} c_{12}c_{13} & s_{12}c_{13} & s_{13}e^{-i\delta} \\ -c_{23}s_{12} - s_{23}c_{12}s_{13}e^{i\delta} & c_{23}c_{12} - s_{23}s_{12}s_{13}e^{i\delta} & s_{23}c_{13} \\ s_{23}s_{12} - c_{23}c_{12}s_{13}e^{i\delta} & -s_{23}c_{12} - c_{23}s_{12}s_{13}e^{i\delta} & c_{23}c_{13} \end{pmatrix} U'_P, \quad (25)$$

$$U'_P = \text{diag}(1, e^{i\alpha_{21}/2}, e^{i\alpha_{31}/2}), \quad (26)$$

where $c_{ij} = \cos \theta_{ij}$, $s_{ij} = \sin \theta_{ij}$ ($ij = 12, 23, 13$), δ and α_{21}, α_{31} are the Dirac and two Majorana CP-violating phases, respectively. Then we can derive, up to the second order of s_{13} , namely $\mathcal{O}(s_{13}^2)$, the lepton mixing angles and CP phases as

$$s_{13} = |U_{e3}| = \sqrt{\frac{2}{3}}s_\theta,$$

$$\begin{aligned}
\delta &= \zeta, \quad \alpha_{21} = \varphi_2 - \varphi_1, \quad \alpha_{31} = \varphi_3 - \varphi_1, \\
s_{12}^2 &= \frac{|U_{e2}|^2}{1 - |U_{e3}|^2} = \frac{1}{3(1 - s_{13}^2)}, \\
s_{23}^2 &= \frac{|U_{\mu 3}|^2}{1 - |U_{e3}|^2} \simeq \frac{1}{2} + \frac{1}{\sqrt{2}} \left(s_{13} - \frac{3}{4} s_{13}^2 \right) c_\delta,
\end{aligned} \tag{27}$$

where the mixing angle θ is obtained as

$$t_{2\theta} = \frac{\sqrt{3}\epsilon\tilde{\kappa}}{(2 + \epsilon)\tilde{\kappa} \cos \zeta - 3i \sin \zeta}. \tag{28}$$

Apart from that, the consistency of the imaginary parts between all elements of the two matrices in Eqs. (24) and (25) results in $\sin \delta = \sin \zeta = 0$, up to the order $\mathcal{O}(s_{13}^2)$. Following this, we hereafter take $\zeta = \pi$ (therefore the Dirac CP phase $\delta = \pi$ which is consistent with its experimental values at 3σ given in Ref. [20]), and then we get

$$t_{2\theta} = \frac{-\sqrt{3}\epsilon}{2 + \epsilon}. \tag{29}$$

As a result, ϵ can be written as a function of s_{13} , namely

$$\epsilon = -\frac{4t_\theta}{t_\theta(2 - \sqrt{3}t_\theta) + \sqrt{3}}, \tag{30}$$

where $t_\theta = s_\theta/c_\theta$ and $s_\theta = \sqrt{3/2}s_{13}$. We note that s_{13} is real, hence ϵ is real too. Combining with the notation given in Eq. (19), the complex parameter $\tilde{\kappa}$ can be written as

$$\tilde{\kappa} = \kappa \times e^{i\phi}, \quad \kappa = |\tilde{\kappa}| > 0. \tag{31}$$

Before coming to the numerical investigation, we would like to give some interesting comments to distinguish our work from previous works. Although the structures of m_D and M_R introduced in our model are slightly different from those in the model given by Ref. [29], the two models have the same small mixing angle θ that has the same relation with s_{13} , namely Eq. (27), leading to similar formulas for s_{12}^2 and s_{23}^2 up to the order $\mathcal{O}(s_{13}^2)$. In addition, θ is determined by Eq. (29), which seems to have the same form as given in Ref. [29], where $\epsilon = -\lambda_1$. However, the important difference is that we have proved that ϵ is real based on Eq. (30), while λ_1 is the modulus of a more general complex parameter. This means that we will scan fewer independent parameters in our numerical calculation. Another difference is that, while $\delta = 0$ is chosen without explanation in Ref. [29], we obtain $\delta = \pi$ from the condition $s_\delta = 0$ mentioned above and the recent neutrino oscillation data.

Based on Eqs. (21), (27), and (29), the three active neutrino masses, the three mixing angles and the Dirac CP phase are explicitly shown in terms of the model parameters m_0, ϵ, κ , and ϕ . At present, we have five experimental results that are taken as inputs in our numerical analysis, given at 3σ by Ref. [20] for the normal hierarchy (NH) of the active neutrino mass spectrum as

$$\begin{aligned} s_{12}^2 &= 0.250 - 0.354; \quad \Delta m_{21}^2 (10^{-5} \text{eV}^2) = 6.93 - 7.96, \\ \Delta m_{31}^2 (10^{-3} \text{eV}^2) &= 2.45 - 2.69, \quad s_{13}^2 = 0.0190 - 0.0240, \\ s_{23}^2 &= 0.381 - 0.615, \quad \delta/\pi(2\sigma) = 1.0 - 1.9, \end{aligned} \quad (32)$$

and for the inverted hierarchy (IH) as (θ_{12} and Δm_{21}^2 are unchanged)

$$\begin{aligned} \Delta m_{23}^2 (10^{-3} \text{eV}^2) &= 2.42 - 2.66, \quad s_{13}^2 = 0.0190 - 0.0242, \\ s_{23}^2 &= 0.384 - 0.636, \quad \delta/\pi(2\sigma) = 0.92 - 1.88. \end{aligned} \quad (33)$$

where $\Delta m_{ij}^2 = m_i^2 - m_j^2$.

We impose the current experimental data of active neutrino masses and mixing angles on the above relations and scan the whole parameter space including the following parameters: $m_0, \epsilon, \kappa, \phi$. In particular, our investigation will try to find the allowed regions of the parameter space that satisfy both the recent experimental data of neutrino oscillation and leptogenesis. Before scanning all allowed regions satisfying 3σ data of neutrino oscillation, we will estimate the scanning ranges of these parameters by fixing s_{13} and Δm_{21}^2 at their best-fit values, while formulating all the other required parameters as functions of κ and ϕ . Because s_{12}^2 , s_{23}^2 , and ϵ can be formulated as functions of only s_{13} , we will investigate them under constraints of recent experimental data of neutrino mixing given in Eqs. (32) and (33). This helps us estimate the allowed ranges of these dependent parameters for further investigation. Plots of s_{12}^2 and s_{23}^2 as functions of s_{13} in the 3σ ranges are shown in Fig. 1, where the dotted and dashed lines show the respective lower and upper bounds of the 3σ allowed ranges given from experimental data. With s_{13} in the 3σ range, all values of s_{12}^2 and s_{23}^2 evaluated from the functions given in Eqs. (32) and (33) always satisfy the 3σ allowed ranges. Hence it is enough to pay attention only to the 3σ constraint of s_{13} . The allowed values of ϵ are presented in Fig. 2.

For s_{13}^2 in the 3σ range, it is easy to derive the allowed values of ϵ ,

$$\text{NH : } \quad -0.376 \leq \epsilon \leq -0.339,$$

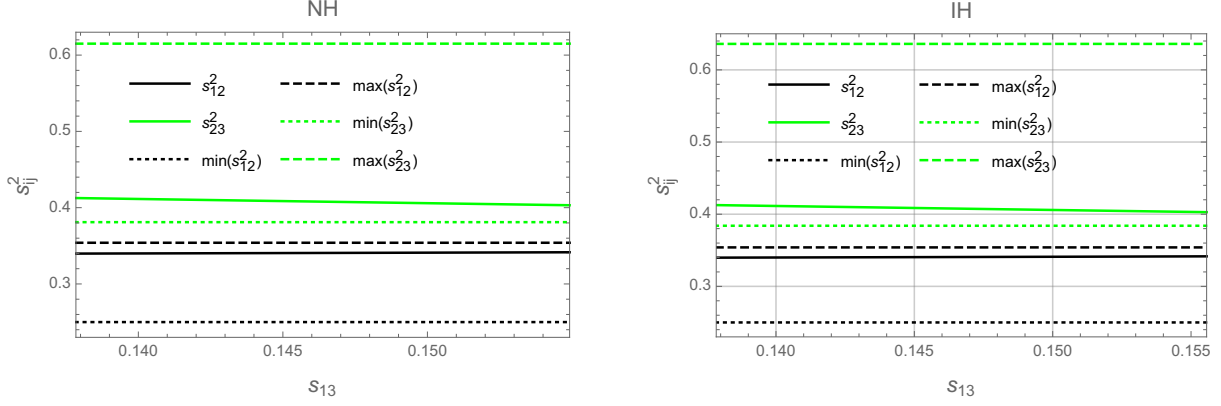


FIG. 1: s_{12}^2 and s_{23}^2 as functions of s_{13} in the left (right) panel for the NH (IH) case.

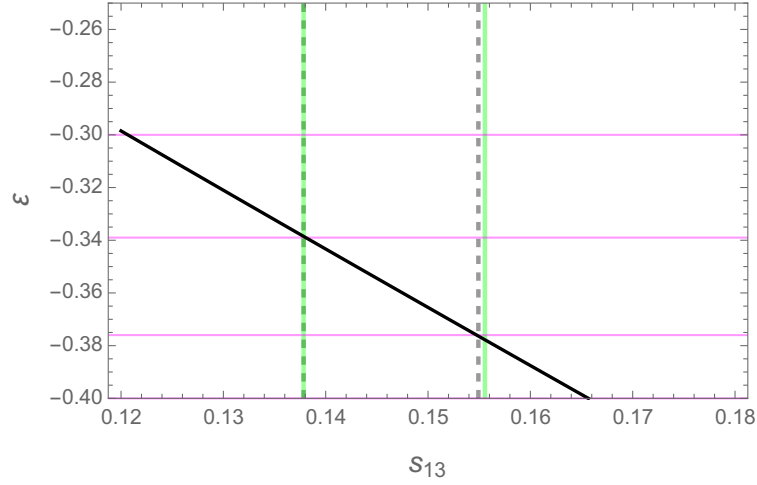


FIG. 2: Plot of ϵ as a function of s_{13} . The two black dashed (blue) vertical lines show the lower and upper bounds of the 3σ ranges of s_{13} corresponding to the NH (IH) case.

$$\text{IH : } -0.378 \leq \epsilon \leq -0.339. \quad (34)$$

At the best-fit point we have $\epsilon = -0.358$ (-0.359) for the NH (IH) case.

To estimate the allowed range of κ and ϕ , we use Eq. (21) to derive m_0 as a function of Δm_{21}^2 , s_{13} and $\tilde{\kappa}$,

$$m_0^2 = \Delta m_{21}^2 \left[\frac{1}{|\tilde{\kappa}(2 + \epsilon)|^2} - \frac{1}{|3/2 - \tilde{\kappa}\sqrt{1 + \epsilon + \epsilon^2}|^2} \right]^{-1}, \quad (35)$$

where ϵ and $\tilde{\kappa}$ are given by Eqs. (30) and (31), respectively. Inserting this form of m_0 into the equations in Eq. (21), we derive $m_{1,2,3}$, Δm_{31}^2 , and Δm_{23}^2 as functions of Δm_{21}^2 , s_{13} , κ , and ϕ . Using the best-fit values of Δm_{21}^2 and s_{13} , we can plot Δm_{31}^2 (Δm_{23}^2) as functions of κ with different fixed ϕ . In Fig. 3, Δm_{31}^2 and Δm_{23}^2 corresponding to the two NH and IH

cases are plotted as functions of κ with different fixed ϕ .

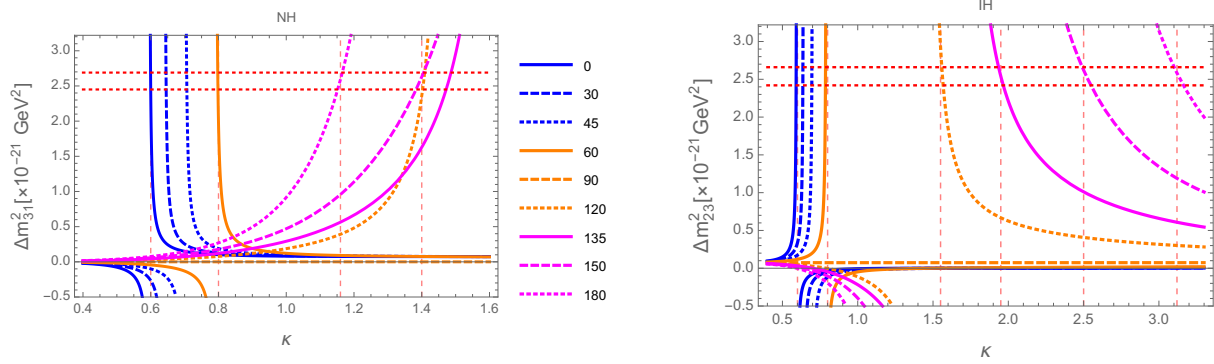


FIG. 3: The left (right) panel presents Δm_{31}^2 (Δm_{23}^2) as a function of κ with different fixed $0^\circ \leq \phi \leq 180^\circ$ in the NH (IH) case. The two red dotted lines show the 3σ allowed range of Δm_{31}^2 (Δm_{23}^2) corresponding to the NH (IH) case.

Here we chose the plot range of ϕ as $0^\circ \leq \phi \leq 180^\circ$ because the results in the range $180^\circ \leq \phi \leq 360^\circ$ are repeated. We see that with every fixed ϕ , the respective allowed range of κ is very narrow. In addition, the two values of $\phi = 90^\circ$ and 270° are ruled out completely for all κ because they always result in $m_1 = m_3$, leading to $\Delta m_{31}^2 = 0$ and $\Delta m_{21}^2 = \Delta m_{23}^2$ ruled out by both the NH and the IH data. The allowed regions divide into three, namely $\kappa < 1$ for $0^\circ \leq \phi < 90^\circ$ and $270^\circ < \phi < 360^\circ$, while $\kappa > 1$ for $90^\circ < \phi < 270^\circ$. In fact, the allowed regions are more strict because they must satisfy an additional condition that the formula of m_0^2 given in Eq. (35) is positive. To see how the condition $m_0^2 > 0$ works, we use the contour plots in Fig. 4 for the NH case, where Δm_{31}^2 , m_0^2 , m_0 , and m_1 are functions of ϕ and $0.6 \leq \kappa < 2$, which is derived from the allowed κ shown in Fig. 3.

We can see in Fig. 4 that the allowed region is divided into two symmetric subregions by the horizontal axis $\phi = 180^\circ$, as mentioned previously. In addition, in each subregion, for example the allowed region with $90^\circ < \phi < 180^\circ$, there exists another symmetric horizontal axis $\phi = 135^\circ$ where two values of $\phi = 135^\circ \pm x^\circ$ will give the same Δm_{31}^2 for one fixed κ . Hence, in Fig. 3 the two lines $\phi = 120^\circ$ and $\phi = 150^\circ$ result in the same Δm_{31}^2 , and the line $\phi = 120^\circ < 135^\circ$ is different from the three others lines $\phi = 180^\circ$, 150° , $135^\circ \geq 135^\circ$.

Now, only the region satisfying $1.15 < \kappa < 1.5$ and $90^\circ < \phi < 270^\circ$ are allowed for the NH case. We also roughly estimate the allowed ranges of m_0 and the lightest active neutrino mass m_1 as $0.035 \text{ eV} < m_0 < 0.25 \text{ eV}$ and $0.002 \text{ eV} < m_1 < 0.03 \text{ eV}$.

In the IH case, illustrations are shown in Fig. 5, where the contour plots are limited in

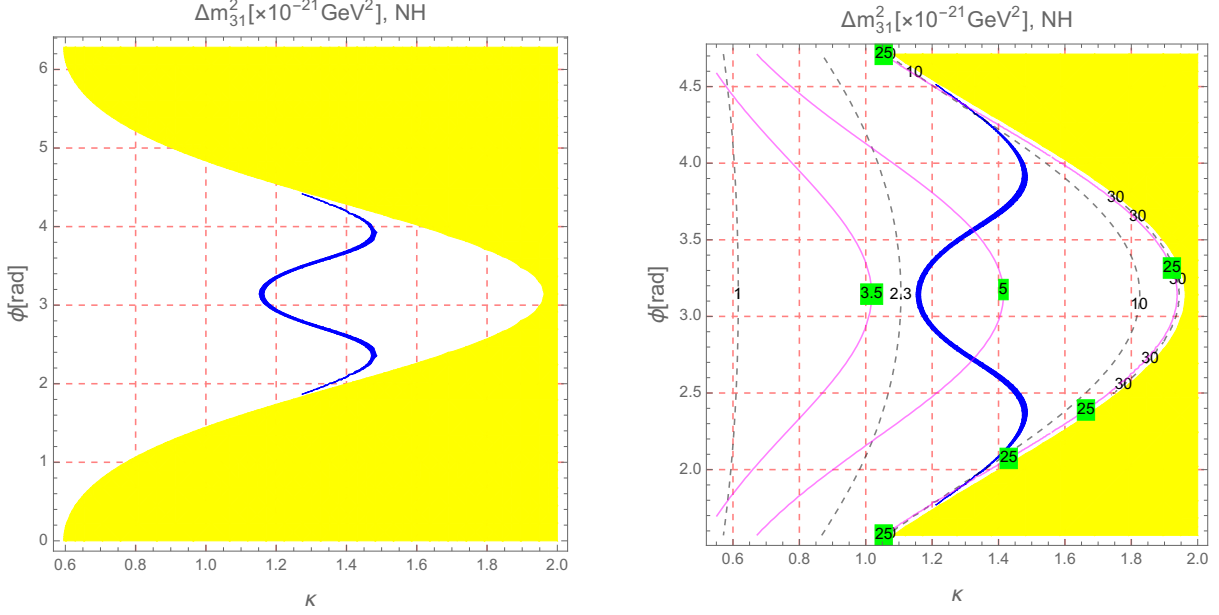


FIG. 4: Contour plots of Δm_{31}^2 as functions of κ and ϕ in the NH case. The blue regions show the 3σ allowed range of Δm_{31}^2 . The yellow regions are excluded by the condition $\Delta m_{21}^2/m_0^2 > 0$. The magenta and black dashed curves in the right panel show the respective constant values of $m_0 \times 10^{11}$ [GeV] and $m_1 \times 10^{12}$ [GeV].

two ranges of $0^\circ \leq \phi \leq 60^\circ$ and $300^\circ < \phi < 360^\circ$.

The allowed regions satisfy that $0.5 < \kappa < 0.8$ and $\phi \in (0^\circ, 90^\circ) \cup (270^\circ, 360^\circ)$. Values of ϕ close to 90° and 270° are excluded. Indeed, the total allowed regions respecting the 3σ allowed range of Δm_{23}^2 correspond to $0^\circ \leq \phi < 90^\circ$ and $270^\circ < \phi < 360^\circ$. Crude estimations of m_0 and m_1 are $0.02 \text{ eV} < m_0 < 0.06 \text{ eV}$ and $0.04 \text{ eV} < m_1 < 0.09 \text{ eV}$.

Particular allowed pairs of (κ, ϕ) are collected in Tables II and III for the NH and the IH cases, respectively. This will be very convenient for investigating the LFV decays later. In the second column of every table, the values of κ are determined at the best-fit value and 3σ range of Δm_{31}^2 (Δm_{23}^2) for the NH (IH) scheme.

Comparing with previous work [29], we can see many new interesting results shown in the numerical estimation here. First, in our new approach, ϵ is investigated as a real function of s_{13} . Consequently, both s_{13}^2 and s_{23}^2 are also written as functions of s_{13} , leading to a very interesting results that these two quantities always satisfy the 3σ ranges. In addition, the constraint of ϵ is determined precisely from the 3σ allowed range of s_{13} . This approach also shows us clearly that the two allowed regions of the pairs (κ, ϕ) corresponding to the two

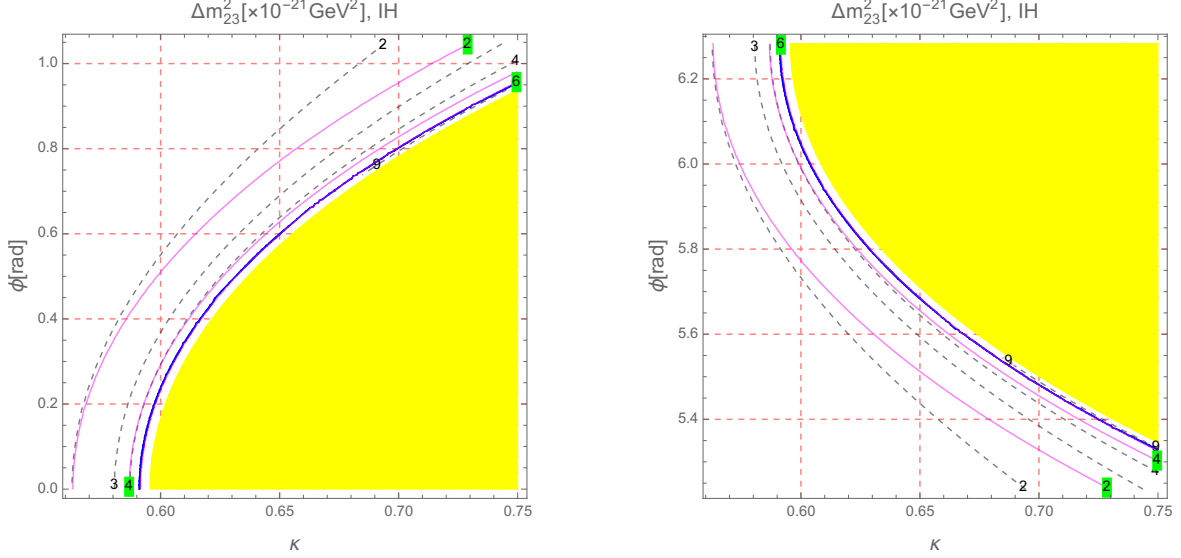


FIG. 5: Contour plots of Δm_{23}^2 as functions of κ and ϕ in the range $0 \leq \phi \leq \pi/3$ (left) and $5\pi/3 \leq \phi \leq 2\pi$ for the IH case. The blue regions show the 3σ allowed range of Δm_{23}^2 . The yellow regions are excluded by the condition $\Delta m_{21}^2/m_0^2 > 0$. The magenta and black dashed curves in the right panel show respective constant values of $m_0 \times 10^{11}$ [GeV] and $m_1 \times 10^{11}$ [GeV].

NH and IH cases are completely distinguished.

From the above discussion, we have shown that by fixing s_{13} and Δm_{21}^2 we can estimate the reasonable ranges of all parameters ϵ , m_0 , κ , and ϕ . This is also consistent with the derivation of m_0 from the seesaw formula $m_0 = \frac{(pv_u)^2}{M_0} \simeq \sqrt{\Delta m_{31(23)}^2} \simeq 0.05$ eV for the best-fit data. We emphasize that, although our first approach for numerical investigation seems similar to that given in Ref. [11], our detailed discussion added more strict conditions for m_0^2 and $\Delta m_{31,23}^2$ to show precisely the allowed ranges of κ and ϕ . More importantly, in the following numerical investigation we will scan the parameter space including four independent parameters (m_0 , ϵ , κ , ϕ) around the ranges that have been estimated above to collect all allowed points which satisfy all of the 3σ experimental data of the NH or the IH cases. This method of investigation is more general than those mentioned in Refs. [11, 29]. Coming back to our numerical investigation, for the NH (IH) the unknown parameters get random values in the following ranges: $0.02 \text{ eV} \leq m_0 \leq 0.15 \text{ eV}$ ($0.05 \text{ eV} \leq m_0 \leq 0.15 \text{ eV}$), $-0.45 \leq \epsilon \leq -0.25$ ($-0.4 \leq \epsilon \leq -0.32$), $1 \leq \kappa \leq 1.7$ ($0.45 \leq \kappa \leq 1.05$), and $0 \leq \phi \leq 2\pi$. Finally, the RHN mass scale and t_β are chosen as $M_0 = 10^{10}$ GeV and $t_\beta = 3$ for the numerical investigation of p , which is the global parameter of the Dirac neutrino Yukawa

TABLE II: Allowed values of (κ, ϕ) generating active neutrino data in 3σ range with fixed values at best-fit points of $s_{13}^2 = 0.0215$ and $\Delta m_{21}^2 = 7.37 \times 10^{-23} \text{GeV}^2$ in the NH case. The best-fit values and allowed ranges of κ corresponding to every fixed ϕ are presented in the column two.

ϕ	κ	Δm_{31}^2	m_0	m_1
[$^\circ$]	best-fit, [allowed range]	$[\times 10^{-21} \text{ GeV}^2]$	$[\times 10^{-11} \text{ GeV}]$	$[\times 10^{-11} \text{ GeV}]$
95	1.1379, [1.1377, 1.1381]	2.5785	22.744	12.143
120	1.4056, [1.4027, 1.4087]	2.5366	8.6036	3.6293
135	1.4788, [1.4720, 1.4863]	2.5593	6.0594	2.3432
150	1.3938, [1.3834, 1.4055]	2.5599	3.9809	1.5129
180	1.1582, [1.1518, 1.1654]	2.5594	2.4929	0.99067
210	1.3938, [1.3834, 1.4055]	2.5599	3.9809	1.5129
225	1.4788, [1.4720, 1.4863]	2.5593	6.0594	2.3432
240	1.4056, [1.4027, 1.4087]	2.5603	8.6447	3.6459
265	1.1379, [1.1377, 1.1381]	2.5601	22.662	12.099

coupling matrix Y_ν roughly estimated by $p^2 \simeq \frac{M_0 \sqrt{\Delta m_{31(23)}^2}}{v_u^2}$.

The parameter spaces (κ, ϵ) and (ϕ, p) are respectively plotted Figs 6 and 7, where the red and blue patterns represent the allowed regions of NH and the IH cases, respectively. Hereafter, we continue using these conventions unless otherwise stated. Note that M_0 and

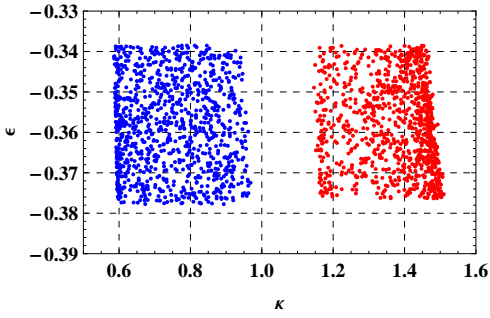


FIG. 6: The allowed values of κ and ϵ of the model. The red and blue patterns correspond to the NH and the IH of active neutrino masses, respectively.

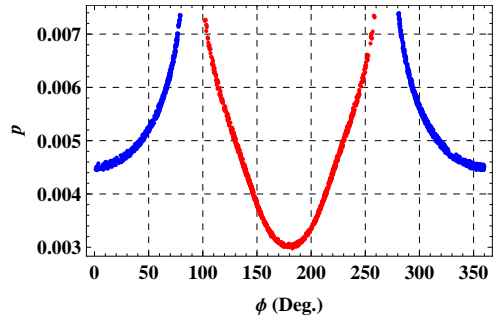


FIG. 7: The correlation between the allowed values of ϕ and the Dirac neutrino coupling factor p of the model. The roles of color patterns are the same as Fig. 6.

TABLE III: Allowed values of (κ, ϕ) generating active neutrino data in 3σ range with fixed values at best-fit points of 0.0216 and $\Delta m_{21}^2 = 7.37 \times 10^{-23} \text{ GeV}^2$ in the IH case.

ϕ	κ	Δm_{23}^2	m_0	m_1
[$^\circ$]	best-fit, [allowed range]	$[\times 10^{-21} \text{ GeV}^2]$	$[\times 10^{-11} \text{ GeV}]$	$[\times 10^{-11} \text{ GeV}]$
10	0.5960, [0.5958, 0.5962]	2.5377	5.6341	5.6958
30	0.6357, [0.6354, 0.6359]	2.6545	6.3001	5.9753
45	0.6953, [0.6950, 0.6956]	2.5293	7.0243	6.0955
60	0.7859, [0.7856, 0.7862]	2.5262	8.6822	6.6763
85	1.0207, [1.0205, 1.0208]	2.5821	22.271	13.267
275	1.0207, [1.0205, 1.0208]	2.5821	22.271	13.267
300	0.7859, [0.7856, 0.7862]	2.5262	8.6822	6.6763
315	0.6953, [0.6950, 0.6956]	2.5293	7.0243	6.0955
350	0.5960, [0.5958, 0.5962]	2.5490	5.6469	5.7088

t_β are absorbed into m_0 by the seesaw formula. As a result, the allowed regions of the parameter spaces plotted in Fig. 6 is independent from the values of t_β and M_0 .

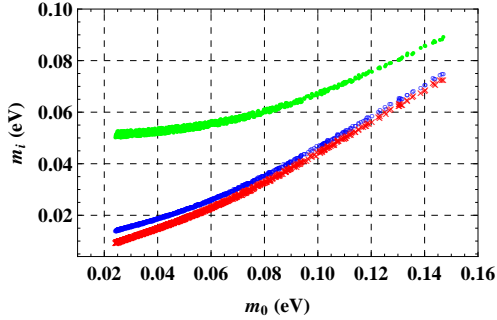


FIG. 8: The active neutrino masses m_i as a function of m_0 for the NH case.

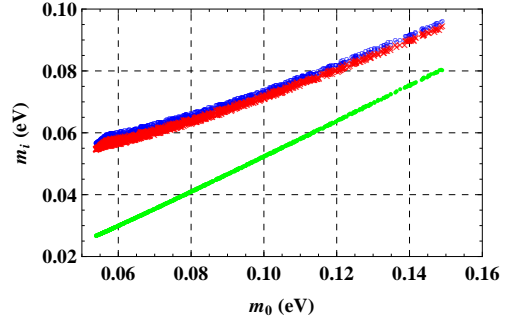


FIG. 9: The active neutrino masses m_i as a function of m_0 for the IH case.

The light neutrino masses predicted by the model are respectively plotted in Figs. 8 and 9, as functions of the light neutrino mass scale m_0 for the NH and IH cases. There, the red, blue, and green plots represent for m_1 , m_2 , and m_3 , respectively.

We can recognize that the neutrino masses are strong hierarchy with small values of m_0 and they can be quasi-degenerate, $m_1 \cong m_2 \cong m_3 \geq 0.1 \text{ eV}$ [20], if m_0 approaches above 0.15 eV. The prediction of the two Majorana CP phases is shown in Fig. 10.

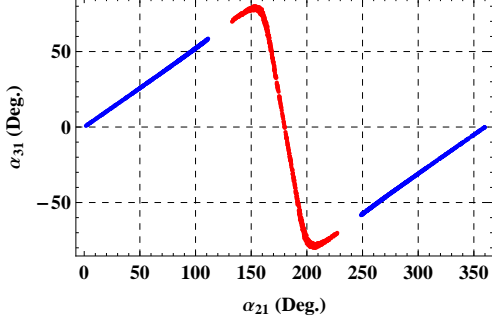


FIG. 10: The predictions of the model for the Majorana CP-violating phases for the NH (red) and the IH (blue) cases.

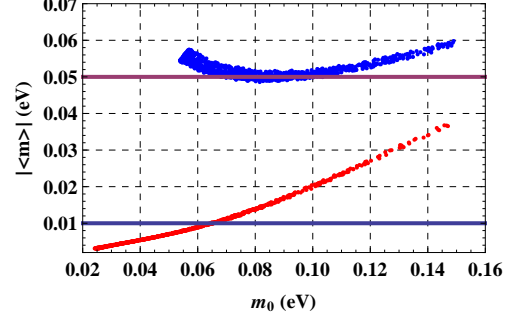


FIG. 11: The predictions of the effective neutrino mass $|\langle m \rangle|$ as a function of the active neutrino mass scale m_0 .

It is worth to studying the effective neutrino mass in neutrinoless double beta decay ($0\nu\beta\beta$), $|\langle m \rangle|$, with the form given in Ref. [20] as

$$\begin{aligned} |\langle m \rangle| &= |m_1(U_{\text{PMNS}})_{e1}^2 + m_2(U_{\text{PMNS}})_{e2}^2 + m_3(U_{\text{PMNS}})_{e3}^2| \\ &= \left| \left(m_1 c_{12}^2 + m_2 s_{12}^2 e^{i\alpha_{21}} \right) c_{13}^2 + m_3 s_{13}^2 e^{i(\alpha_{31}-2\delta)} \right|. \end{aligned} \quad (36)$$

The prediction of the effective mass $|\langle m \rangle|$ is plotted in Fig. 11 as a function of the lightest active neutrino mass m_0 for the NH (red plot) and IH (blue plot) cases. In this figure, the two horizontal lines are the prospect bounds for $|\langle m \rangle|$ of a new generation of $0\nu\beta\beta$ experiments [20]. Numerically, our predictions of $|\langle m \rangle|$ turn out to be $0.002 \text{ eV} \leq |\langle m \rangle| \leq 0.038 \text{ eV}$ for NH and $0.048 \text{ eV} \leq |\langle m \rangle| \leq 0.058 \text{ eV}$ for IH. Notice that the results from $0\nu 2\beta$ by KamLAND-Zen [46] and EXO-200 [47] indicate an upper limit on the effective neutrino mass parameter $|\langle m \rangle|$ that $|\langle m \rangle| \leq (0.14 - 0.28) \text{ eV}$ at 90% CL. and $|\langle m \rangle| \leq (0.19 - 0.45) \text{ eV}$ at 90% CL., respectively. The most stringent upper limit now is $|\langle m \rangle| \leq (0.061 - 0.165) \text{ eV}$ at 90% CL [48]. Therefore, our result for $|\langle m \rangle|$ is still not excluded by the current experimental bounds, and we expect that our predictions for $|\langle m \rangle|$ could be measured by KamLAND-Zen and other $0\nu 2\beta$ decay experiments in their new phase which have been taking data since mid 2017; see, for the present status and future prospects, Ref. [49]. The future sensitivity can reach $|\langle m \rangle| = 0.01 \text{ eV}$; see a summary in Ref. [50], where the sensitivity of many ongoing and planned $0\nu\beta\beta$ experiments [47, 51–63] were listed. Because the two ranges of $|\langle m \rangle|$ predicted by the NH and IH cases are completely distinguished, $|\langle m \rangle|$ is an important channel to confirm experimentally the NH or the IH property once the effective mass $|\langle m \rangle|$ is measured. In addition, we can pin down the light neutrino mass scale m_0 and

either of the active neutrino masses.

To finish the numerical investigation, we conclude some important constraints on the model parameters. The allowed ranges of the four parameters $(m_0, \epsilon, \kappa, \phi)$ are constrained as follows. The allowed regions for the NH case are: $0.02 \text{ eV} < m_0 < 0.15 \text{ eV}$, $-0.038 < \epsilon < -0.0345$, $1.15 < \kappa < 1.5$, and $90^\circ < \phi < 270^\circ$. The allowed regions for the IH case are: $0.05 \text{ eV} < m_0 < 0.15 \text{ eV}$, $-0.038 < \epsilon < -0.0345$, $0.55 < \kappa < 1$, $0^\circ < \phi < 90^\circ$, and $270^\circ < \phi < 360^\circ$. In addition, the allowed region of the light neutrino mass scale m_0 lead to upper bounds of M_0 obtained from the perturbative limit: $M_0 = (v_u^2 p)/m_0 \leq 174^2 \times 4\pi/(0.02 \times 10^{-11}) \sim O(10^{16}) \text{ GeV}$. This is consistent with the GUT scale mentioned in this work.

Interestingly enough, in the next section we would like to study how the BAU can be explained by the leptogenesis scenario of the current model under the allowed regions of the parameter space discussed in this section.

III. LEPTOGENESIS

We now consider how leptogenesis can work in our scenario. The relations between heavy RHNs and active neutrino masses are derived directly from Eq. (20),

$$U_R^T M_R U_R = \text{diag}(M_1, M_2, M_3) = (v_u p)^2 \text{diag}\left(\frac{1}{m_1}, \frac{1}{m_2}, \frac{1}{m_3}\right), \quad (37)$$

where $U_R = U_{\text{PMNS}}^*$ was determined precisely in the previous section. In the mass basis of the RHNs, the Dirac neutrino Yukawa coupling matrix is modified to be

$$Y'_\nu = U_R^T Y_\nu = U_{\text{PMNS}}^\dagger Y_\nu \Rightarrow H = Y'_\nu Y_\nu'^\dagger = p^2 \times \mathbf{1}. \quad (38)$$

We study the case of flavored leptogenesis, the CP asymmetry in the decay of RHN N_i to lepton flavor l_α ($\alpha = e, \mu, \tau$) is defined as [64–70]

$$\begin{aligned} \varepsilon_i^\alpha &= \frac{\Gamma(N_i \rightarrow l_\alpha \varphi) - \Gamma(N_i \rightarrow \bar{l}_\alpha \varphi^\dagger)}{\sum_\alpha [\Gamma(N_i \rightarrow l_\alpha \varphi) + \Gamma(N_i \rightarrow \bar{l}_\alpha \varphi^\dagger)]} \\ &= \frac{1}{8\pi H_{ii}} \sum_{j \neq i} \left\{ \text{Im} \left[H_{ij} (Y'_\nu)_{i\alpha} (Y'_\nu)_{j\alpha}^* \right] f\left(\frac{M_j^2}{M_i^2}\right) \right\}, \end{aligned} \quad (39)$$

where $H = Y'_\nu Y_\nu'^\dagger$, and M_i denotes the RHN masses. The loop function $f(x)$ containing the vertex and self-energy corrections is given as

$$f(x) = \sqrt{x} \left[(1+x) \ln \frac{x}{1+x} + \frac{2-x}{1-x} \right]. \quad (40)$$

Notice from Eq.(39) that, in the original model, the CP asymmetry is zero due to the fact that the Hermitian matrix H is proportional to the unit matrix, see Eq. (38), and a non-vanishing CP asymmetry requires $\text{Im}[H_{ij}(Y'_\nu)_{i\alpha}(Y'_\nu)^*_{j\alpha}] \neq 0$. Therefore, to have leptogenesis we need to induce a non-vanishing H_{ij} ($i \neq j$) at the leptogenesis scale. Indeed, this happens in the model under consideration because of the RG (renormalization group) effects, discussed in detail below. The RG equation for the Dirac neutrino Yukawa coupling can be written as [71–75]

$$\frac{dY_\nu}{dt} = Y_\nu \left[\left(T - \frac{3}{4}g_2^2 - \frac{9}{4}g_1^2 \right) - \frac{3}{2} \left(Y_l^\dagger Y_l - Y_\nu^\dagger Y_\nu \right) \right], \quad (41)$$

where $T = \text{Tr}(3Y_u^\dagger Y_u + 3Y_d^\dagger Y_d + Y_\nu^\dagger Y_\nu + Y_l^\dagger Y_l)$, $Y_{u,d}$ and Y_l are the Yukawa couplings of up-type and down-type quarks and charged leptons, $g_{2,1}$ are the $\text{SU}(2)_L$ and $\text{U}(1)_Y$ gauge coupling constants, respectively, $t = \frac{1}{16\pi^2} \ln(M/\Lambda')$, and M is an arbitrary renormalization scale. The cutoff scale Λ' can be regarded as the G_f breaking scale $\Lambda' = \Lambda$ and is assumed to be of the order of the GUT scale, $\Lambda' \sim 10^{16}$ GeV.

As the structure of M_R changes with the evolution of the energy scale, U_R depends on the scale Λ' too. The RG evolution of $U_R(t)$ can be written as

$$\frac{d}{dt}U_R = U_R A, \quad (42)$$

where A is an anti-Hermitian matrix $A^\dagger = -A$ due to the unitarity of U_R . The components of the A matrix are given by [76]

$$A_{ij} = \frac{M_j + M_i}{M_j - M_i} \text{Re}[(Y_\nu Y_\nu^\dagger)_{ij}] + i \frac{M_j - M_i}{M_j + M_i} \text{Im}[(Y_\nu Y_\nu^\dagger)_{ij}]. \quad (43)$$

The running of the RHN mass scale affects very weakly our result so we drop it here. The RG equation for Y'_ν in the basis of diagonal M_R is then obtained as

$$\frac{dY'_\nu}{dt} = Y'_\nu \left[\left(T - \frac{3}{4}g_2^2 - \frac{9}{4}g_1^2 \right) - \frac{3}{2} \left(Y_l^\dagger Y_l - Y_\nu'^\dagger Y'_\nu \right) \right] + A^T Y'_\nu. \quad (44)$$

Finally, we obtain the RG equation for the Hermitian matrix $H = Y'_\nu Y_\nu'^\dagger$ responsible for the leptogenesis as

$$\frac{dH}{dt} = 2 \left(T - \frac{3}{2}g_2^2 - \frac{9}{4}g_1^2 \right) H - 3Y_\nu(Y_l^\dagger Y_l)Y_\nu'^\dagger + 3H^2 + A^T H + H A^*. \quad (45)$$

With the Hermitian matrix H given in Eq. (38), up to non-zero leading contributions in the right-hand side of Eq. (45), the RG is generated from the off-diagonal terms of the H

matrix as

$$H_{ij}(t) \simeq -3y_\tau^2(Y'_\nu)_{i3}(Y'_\nu)^*_{j3} \times t. \quad (46)$$

The flavored CP asymmetries ε_i^α can then be obtained. Notice that, in this model, the tau Yukawa coupling constant (y_τ) relates to that in the SM ($y_{\tau,\text{SM}}$) as $y_\tau^2 = y_{\tau,\text{SM}}^2(1 + t_\beta^2)$. This enhances the CP asymmetries as $\varepsilon_i^\alpha \sim (1 + t_\beta^2)$, we will later discuss the effect of different values of t_β on the numerical generation of the BAU.

After the CP asymmetry in the decay of N_i , ε_i^α , are calculated, the final value of η_B can be calculated by solving the flavor-dependent Boltzmann equations (BE). These describe the out-of-equilibrium processes such as the decay, inverse decay, and scattering involving the RHNs, as well as the non-perturbative sphaleron interaction. Besides the CP asymmetries ε_i^α , the final value of BAU also depends on the wash-out factors K_i^α which measure the effects of the inverse decay of Majorana neutrino N_i into the lepton flavor α and scalars. The parameter K_i^α is defined as [64]

$$K_i^\alpha = \frac{\Gamma_i^\alpha}{H(M_i)} = (Y'_\nu)_{\alpha i}(Y'_\nu)_{i\alpha} \frac{v_u^2}{m_* M_i}, \quad (47)$$

where Γ_i^α is the partial decay width of N_i into the lepton flavors and Higgs scalars; $H(M_i)$ is the Hubble parameter at temperature $T = M_i$ defined as $H(M_i) \simeq (4\pi^3 g_*/45)^{\frac{1}{2}} M_i^2/M_{\text{Pl}}$, where $M_{\text{Pl}} = 1.22 \times 10^{19}$ GeV is the Planck mass, $g_* \simeq 116$ is the effective number of degrees of freedom of the SM with two Higgs doublets, and the equilibrium neutrino mass $m_* \simeq 10^{-3}$ eV.

Due to the flavor effects, each CP asymmetry ε_i^α contributes differently to the final formula for the baryon asymmetry as [64, 77, 78]

$$\eta_B \simeq -2 \times 10^{-2} \sum_{N_i} \left[\varepsilon_i^e \kappa_i^e \left(\frac{151}{179} K_i^e \right) + \varepsilon_i^\mu \kappa_i^\mu \left(\frac{344}{537} K_i^\mu \right) + \varepsilon_i^\tau \kappa_i^\tau \left(\frac{344}{537} K_i^\tau \right) \right] \quad (48)$$

if the RHN mass is about $M_i \leq (1 + t_\beta^2) \times 10^9$ GeV where the μ and τ Yukawa couplings are in equilibrium and all the flavors are to be treated separately. If $(1 + t_\beta^2) \times 10^9$ GeV $\leq M_i \leq (1 + t_\beta^2) \times 10^{12}$ GeV where only the τ Yukawa coupling is in equilibrium and treated separately while the e and μ flavors are indistinguishable, then the baryon asymmetry is obtained as

$$\eta_B \simeq -2 \times 10^{-2} \sum_{N_i} \left[\varepsilon_i^e \kappa_i^e \left(\frac{417}{589} K_i^e \right) + \varepsilon_i^\tau \kappa_i^\tau \left(\frac{390}{589} K_i^\tau \right) \right], \quad (49)$$

where $\varepsilon_i^2 = \varepsilon_i^e + \varepsilon_i^\mu$ and $K_i^2 = K_i^e + K_i^\mu$. In Eqs. (48) and (49), the wash-out factors κ_i^α are defined as

$$\kappa_i^\alpha \simeq \left(\frac{8.25}{K_i^\alpha} + \left(\frac{K_i^\alpha}{0.2} \right)^{1.16} \right)^{-1}. \quad (50)$$

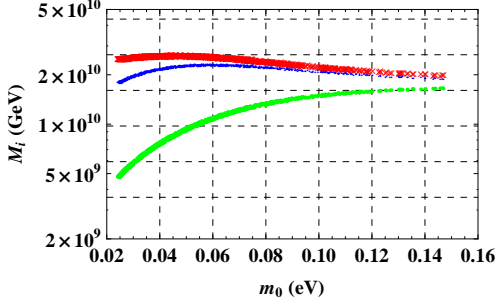


FIG. 12: The RHN masses as functions of the light neutrino mass scale m_0 for the NH with $M_0 = 10^{10}$ GeV.

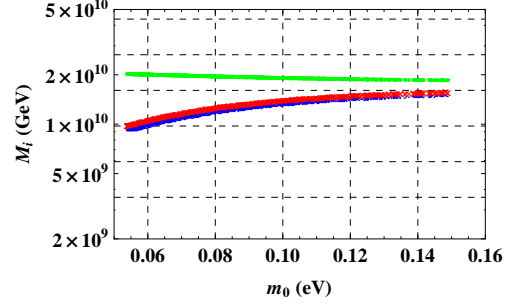


FIG. 13: The RHN masses as functions of the light neutrino mass scale m_0 for the IH with $M_0 = 10^{10}$ GeV.

The allowed regions of parameter space given in Sect. II and all the formulas discussed above for η_B are enough to allow us to investigate numerically the BAU predicted by the model under consideration. For $\tan \beta$ given in Eq. (5), the Lagrangian in Eq. (2) gives $v_u > m_t/\sqrt{4\pi}$. Combining with the relation in Eq. (9), it can be shown easily that $\tan \beta \geq 0.3$, which will be used in the following numerical investigations. First, the mass spectra of RHN masses as functions of the active neutrino mass scale, m_0 , are plotted in Figs. 12 and 13 for the respective NH and the IH cases, where the red, blue, and green lines represent for M_1 , M_2 and M_3 , respectively. Those RHN masses are a strong hierarchy with small values of m_0 and gradually become quasi-degenerate when m_0 approaches values around 0.15 eV. This enhances the generated η_B by the so-called resonant leptogenesis [79].

Later, we can find in Figs. 16 and 17 that η_B increases with increasing m_0 due to the effects of resonant leptogenesis. This is numerically proved in Fig. 14, where the prediction of η_B as a function of the phase ϕ is shown. In this figure, η_B gets two maxima around $\phi = 90^\circ$ and $\phi = 270^\circ$ for both cases of hierarchy of neutrino masses. The reason is that the parameter p of the Y_ν matrix is proportional to $\sqrt{m_0}$, which has two maxima around $\phi = 90^\circ$ and $\phi = 270^\circ$ for both hierarchies (see, Fig. 7). Therefore, m_0 , and hence η_B , also get their maxima around these values of the phase ϕ . In this figure (and in Figs. 15–17),

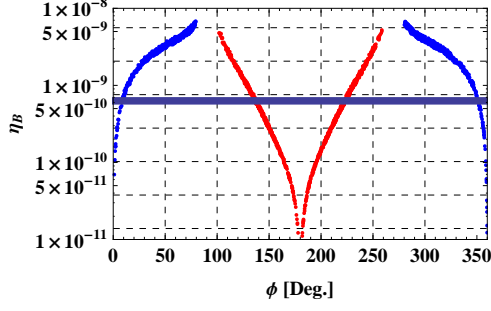


FIG. 14: The prediction of η_B as a function of ϕ , where $t_\beta = 3$ and $M_0 = 10^{10}$ GeV are used. The red (blue) curve represents the NH (IH) case.

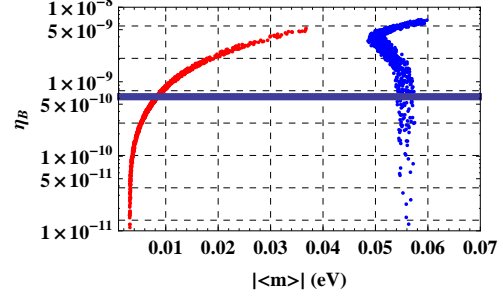


FIG. 15: The correlation between η_B and $|\langle m \rangle|$, where $t_\beta = 3$ and $M_0 = 10^{10}$ GeV are used. The red (blue) curve represents the NH (IH) case.

the solid horizontal bar represents the allowed range from experiment for BAU, namely $\eta_B = (6.3 \pm 0.3) \times 10^{-10}$ [80].

The correlation between η_B and $|\langle m \rangle|$ is shown in Fig. 15 for $M_0 = 10^{10}$ GeV and $t_\beta = 3$, where the red (blue) curve represents the NH (IH) case. As indicated in the previous section, once the exact value of $|\langle m \rangle|$ is confirmed we can point out the active neutrino mass scale m_0 and then we can find out the required values of the RHN mass in order to generate the right amount of η_B for some given values of t_β .

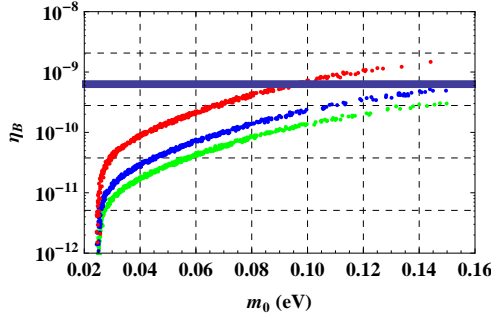


FIG. 16: The prediction of η_B for the case of NH as a function of the active neutrino mass scale m_0 with $M_0 = 10^8$ GeV. The green, blue and red plots correspond to $\tan \beta = 1, 3, 10$, respectively.

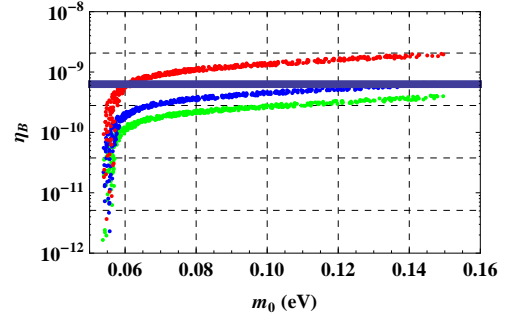


FIG. 17: The prediction of η_B for the case of IH as a function of the active neutrino mass scale m_0 with $M_0 = 10^8$ GeV. The green, blue and red plots correspond to $\tan \beta = 1, 3, 10$, respectively.

The effects of different values of t_β on the resultant of the η_B are shown in Fig. 16 for NH and Fig. 17 for IH. In these figures, the green, blue, and red plots correspond to $t_\beta = 1, 3$ and 10, respectively, with the mass scale of RHN $M_0 = 10^8$ GeV. We can find that η_B

increases with increasing t_β ; with $t_\beta = 3$ the minimum value of the mass scale M_0 is about 10^8 GeV for successful leptogenesis, where the minimum values of M_0 for attaining the right value of η_B are much reduced with larger values of t_β .

We emphasize one important point about the constraint of the heavy neutrino mass scale. For $1 \leq t_\beta \leq 10$, our numerical investigation shows that the constraint is $O(10^8)$ GeV $\leq M_0 \leq O(10^{12})$ GeV in order to successfully generate leptogenesis; see the illustration in Fig. 18. This result can be explained by the fact that M_0 relates to m_0 , p , and $v_u = 174s_\beta$

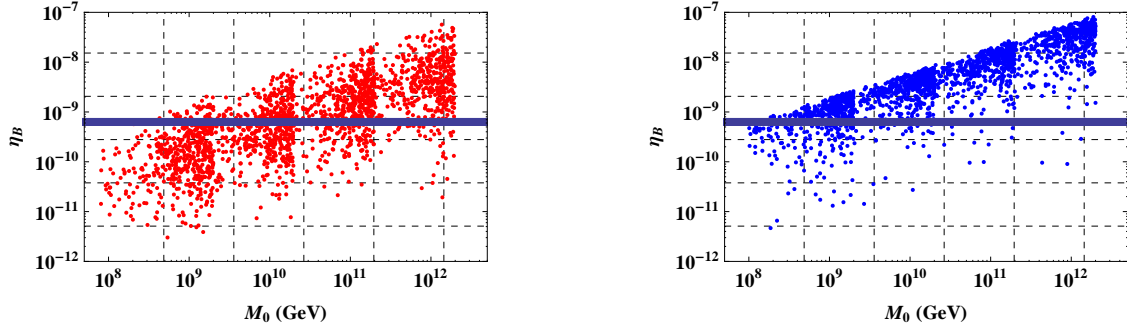


FIG. 18: The prediction of η_B for the case of NH (IN) as a function of the RHN mass scale M_0 with $t_\beta = 3$ in the left (right) panel. The allowed ranges of κ , ϵ , ϕ , and m_0 summarized at the end of Sect. II are used.

through the relation in Eq. (22), where $p \leq \sqrt{4\pi}$ and the allowed m_0 is bounded as mentioned in the previous section. Our investigation shows that successful leptogenesis explained by pure RG effects requires a lower range of the RHN mass scale M_0 than other effects discussed previously, which prefer $M_0 \geq \mathcal{O}(10^{13})$ GeV [11, 29]. Therefore, the scale M_0 may be a clue to understanding which source among RG, NLO, and softterm broken A_4 successfully generates the BAU data.

Recent investigation of the SS models that can generate consistent BAU data suggest that the RHN neutrino mass scale prefers the range below $\mathcal{O}(10^8)$ GeV [81, 82]. The RHN scale is very interesting information to confirm which are the dominant sources generating consistent BAU data.

IV. LEPTON FLAVOR VIOLATING DECAYS $e_b \rightarrow e_a \gamma$

In this section we study the effects of the allowed regions of parameter space satisfying leptogenesis on LFV decays. Neutrino mixing is the only source of LFV processes. The left-

and right-handed bases of the original neutral neutrinos are denoted as $\nu'_L = (\nu_L, (N_R)^c)^T$, where $\nu_L = (\nu_{1L}, \nu_{2L}, \nu_{3L})^T$ and $(N_R)^c = ((N_{1R})^c, (N_{2R})^c, (N_{3R})^c)^T$. Also, we have $\nu'_R = (\nu'_L)^c = ((\nu_L)^c, N_R)^T$. A four-component spinor for a Majorana neutrino is then $\psi = (\psi_L, \psi_R)^T$, where $\psi = \nu_a, N_a$; $\psi_L = \nu_{aL}, (N_{aR})^c$; and $\psi_R = (\nu_{aL})^c, N_{aR}$. They satisfy $\psi^c = C\bar{\psi}^T = \psi$. The relations between a Majorana neutrino and the left- and right-handed components are $\psi_{L,R} = P_{L,R}\psi$, where $P_{L,R} = (1 \mp \gamma_5)/2$. The total mass matrix of the neutrino is

$$M^\nu = \begin{pmatrix} 0 & m_D \\ m_D^T & M_R \end{pmatrix}, \quad (51)$$

where m_D and M_R are given in Eqs. (10) and (15), respectively. The Lagrangian part describing the neutrino mass term is $-\frac{1}{2}\bar{\nu}'_L M^\nu (\nu'_L)^c + \text{H.c.}$ The mass matrix in Eq. (51) is diagonalized by the mixing matrix U^ν , which is unitary and satisfies

$$U^{\nu T} M^\nu U^\nu = \hat{M}^\nu = \text{diag}(m_{n_1}, m_{n_2}, \dots, m_{n_6}) \simeq \text{diag}(m_1, m_2, m_3, M_1, M_2, M_3), \quad (52)$$

where the first three mass values m_{n_a} ($a = 1, 2, 3$) and respective eigenvectors n_a are identified with those of active neutrinos observed by experiments. The remaining masses belong to three heavy neutrinos $n_{4,5,6}$. Hence, the last term in Eq. (52) is derived from the relations shown in Eqs. (13) and (16). The relations between the original and mass basis of the neutrino are

$$\nu'_{iL} = U_{ij}^{\nu*} n_{jL} = U_{ij}^{\nu*} P_L n_j, \quad \nu'_{iR} = U_{ij}^\nu n_{jR} = U_{ij}^\nu P_R n_j, \quad (53)$$

where $n = (n_1, n_2, \dots, n_6)^T$ and $n_i = (n_{iL}, n_{iR})^T$ ($i = 1, 2, \dots, 6$).

Based on previous parameterizations [84, 97], the matrix U^ν can be written as

$$U^\nu = \begin{pmatrix} I_3 & \mathbf{O} \\ \mathbf{O} & U_R \end{pmatrix} \exp \begin{pmatrix} \mathbf{O} & R \\ -R^\dagger & \mathbf{O} \end{pmatrix} \begin{pmatrix} U_{\text{PMNS}} & \mathbf{O} \\ \mathbf{O} & V_3 \end{pmatrix}, \quad (54)$$

where \mathbf{O} is the 3×3 matrix with all elements being zeros; U_R , V_3 , and U_{PMNS} are three 3×3 unitary matrices; and R is a 3×3 matrix satisfying $|R| \equiv \max[|R_{ij}|] \ll 1$ for all $i, j = 1, 2, 3$. Apart from Eq. (12), other SS relations for determining R and heavy neutrino masses are identified up to $\mathcal{O}(R^2)$ as follows

$$R^* = (m_D U_R) [U_R^T M_N U_R]^{-1},$$

$$V_3^* \hat{M}_R V_3 = U_R^T M_N U_R + \frac{1}{2} R^T R^* U_R^T M_N U_R + \frac{1}{2} U_R^T M_N U_R R^\dagger R, \quad (55)$$

where we have applied the result from Refs. [84, 97], after taking a rotation of M^ν corresponding to the first matrix in the right-hand side of Eq. (54), which gives $m_D \rightarrow m_D U_R$ and $M_R \rightarrow U_R^T M_R U_R$.

In our framework, U_R is defined from Eq. (16), and $U_{\text{PMNS}} = U_R^*$ is the well-known mixing matrix of active neutrinos defined in Eq. (24). Therefore, it can be proved that

$$\begin{aligned} R^* &= \sqrt{\frac{m_0}{M_0}} U_{\text{PMNS}}^* \times \text{diag} \left(\frac{M_0}{M_1}, \frac{M_0}{M_2}, \frac{M_0}{M_3} \right), \\ V_3^* \hat{M}_R V_3 &= \text{diag}(M_1, M_2, M_3) + \frac{m_0}{2} \times \text{diag} \left(\frac{M_0}{M_1}, \frac{M_0}{M_2}, \frac{M_0}{M_3} \right) U_{\text{PMNS}} U_{\text{PMNS}}^* \\ &\quad + \frac{m_0}{2} \times U_{\text{PMNS}}^* U_{\text{PMNS}} \text{diag} \left(\frac{M_0}{M_1}, \frac{M_0}{M_2}, \frac{M_0}{M_3} \right). \end{aligned} \quad (56)$$

In the allowed region we have $\mathcal{O}(10^{-11} \text{ GeV}) \sim m_0 \ll M_{1,2,3}$, $M_{1,2,3} \geq \mathcal{O}(10^6) \text{ GeV}$, and $M_0/M_{1,2,3} = \mathcal{O}(1)$, and hence the assumption mentioned above that heavy neutrino masses are given by Eq. (16) is acceptable with a very high accuracy. Using this approximation we also get $V_3 = I_3$.

Up to the order $\mathcal{O}(R^2)$, the mixing matrix U^ν is now

$$U^\nu \simeq \begin{pmatrix} (1 - \frac{1}{2} R R^\dagger) U_{\text{PMNS}} & R \\ -U_{\text{PMNS}}^* R^\dagger U_{\text{PMNS}} & U_{\text{PMNS}}^* (1 - \frac{1}{2} R^\dagger R) \end{pmatrix} + \mathcal{O}(R^3). \quad (57)$$

Finally, U^ν can be presented as a function of M_0 , m_0 , ϕ and κ . As we know, in the minimal model (MSS), where only heavy Dirac neutrinos are added in the SM to explain the neutrino oscillation data, the branching ratio (Br) of the LFV decay $\text{Br}(e_b \rightarrow e_a \gamma)$ was shown to be suppressed, for example $\text{Br}(\mu \rightarrow e \gamma) \leq \mathcal{O}(10^{-54})$. On the other hand, some SM extensions with heavy neutrinos obeying the SS mechanism [31–35] can give large $\text{Br}(e_b \rightarrow e_a \gamma)$, close to the recent experimental sensitivities [85]. In our model, the presence of the charged Higgs boson gives another one-loop contribution to the LFV decay amplitude. This leads to a different prediction for LFV decays that deserves to be investigated. It should be noted that, although in the model under consideration the properties of the charged Higgs boson may be the same as those discussed thoroughly in Refs. [86, 87], the LFV couplings with neutrinos particularly, the behaviors of the LFV may be more predictive than the results of an LFV investigation for 2HDM discussed recently in Ref. [88].

In the Yukawa Lagrangian part of Eq. (1), couplings relating to LFV decays are

$$-\mathcal{L} \rightarrow \frac{m_{e_a}}{\sqrt{2}v_d} S_d \bar{e}_a e_a + \frac{m_{e_a}}{v_d} (\bar{\nu}_{La} e_{Ra} H_d^+ + \text{H.c.})$$

$$+\frac{S_u}{\sqrt{2}}p(\bar{\nu}_{aL}N_{Ra}+\text{h.c.})+p[H_u^-\bar{e}_{aL}N_{Ra}+\text{H.c.}]. \quad (58)$$

Using the transformations to the physical states of the charged Higgs boson and neutrinos given respectively in Eqs. (53) and (4), the Feynman rules for LFV couplings of the charged Higgs boson are collected in Table IV. The Feynman rules for LFV coupling relating with the W boson using our notation can be found in Ref. [89]. They are consistent with those mentioned in 2HDMs [86]. All the Feynman rules for calculating amplitudes of LFV decays $e_b \rightarrow e_a \gamma$ in the unitary gauge are shown in Table IV. Accordingly, the one-loop calculations in this work will be done in the unitary gauge.

TABLE IV: Couplings relating with one-loop three-point Feynman diagrams that contribute to the LFV decay $e_i \rightarrow e_j \gamma$ in the unitary gauge.

Vertex	Coupling	Vertex	Coupling
$\bar{e}_a n_i \varphi^-$	$\frac{-igU_{ai}^{\nu*}}{m_W\sqrt{2}}(m_{e_a}t_\beta P_L + m_{n_i}t_\beta^{-1}P_R)$	$\bar{n}_i e_a \varphi^+$	$\frac{-igU_{ai}^\nu}{m_W\sqrt{2}}(m_{e_a}t_\beta P_R + m_{n_i}t_\beta^{-1}P_L)$
$\bar{e}_a n_i W_\mu^-$	$\frac{ig}{\sqrt{2}}U_{ai}^{\nu*}\gamma^\mu P_L$	$\bar{n}_i e_a W_\mu^+$	$\frac{ig}{\sqrt{2}}U_{ai}^\nu\gamma^\mu P_L$

The Br of the LFV decays $e_b \rightarrow e_a \gamma$ ($m_{e_b} > m_{e_a}$), where $(e_b, e_a) = \{(\tau, \mu), (\tau, e), (\mu, e)\}$, can be determined as follows [90]:

$$\text{Br}(e_b \rightarrow e_a \gamma) = \left(1 - \frac{m_a^2}{m_b^2}\right)^3 \times \frac{12\pi^2}{G_F^2 m_b^2} (|C_L|^2 + |C_R|^2) \times \text{Br}(e_b \rightarrow e_a \bar{\nu}_a \nu_b), \quad (59)$$

where $C_{L,R}$ are scalar factors arising from loop corrections. In the unitary gauge, one-loop Feynman diagrams contributing to $C_{L,R}$ are shown in Fig. 19.

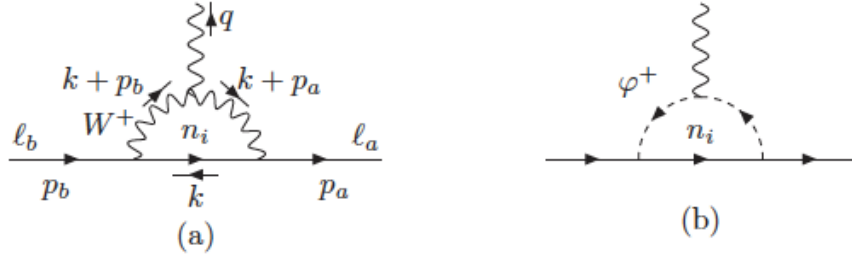


FIG. 19: One-loop Feynman diagrams contributing to $C_{L,R}$ for the decay $e_b \rightarrow e_a \gamma$ in the unitary gauge.

The Br of the decay can therefore be calculated through the well-known decay rates τ or μ , namely $\text{Br}(e_b \rightarrow e_a \bar{\nu}_a \nu_b)$. The corresponding partial decay width is $\Gamma(e_b \rightarrow e_a \bar{\nu}_a \nu_b) = \frac{G_F^2 m_b^5}{192\pi^3}$

with $G_F = \frac{g^2\sqrt{2}}{8m_W^2}$. The experimental values are $\text{Br}(\tau \rightarrow \mu\bar{\nu}_\mu\nu_\tau) \simeq 17.41\%$, $\text{Br}(\tau \rightarrow e\bar{\nu}_e\nu_\tau) \simeq 17.83\%$, and $\text{Br}(\mu \rightarrow e\bar{\nu}_e\nu_\mu) \simeq 100\%$.

In the limit of zero external momenta $m_W^2, m_\varphi^2 \gg p_a^2, p_b^2 \rightarrow 0$, the analytic expressions of the amplitude are

$$C_{L,R} = C_{L,R}^W + C_{L,R}^\varphi, \quad (60)$$

where $C_{L,R}^W$ and $C_{L,R}^\varphi$ are determined in Appendix C, consistent with Ref. [90]. For low energy, Eq. (59) can be written in a more convenient form as

$$\text{Br}(e_b \rightarrow e_a \gamma) = \left(1 - \frac{m_a^2}{m_b^2}\right)^3 \times \frac{3\alpha_e}{2\pi} \left(\frac{m_a^2}{m_b^2} |D_L|^2 + |D_R|^2\right) \times \text{Br}(e_b \rightarrow e_a \bar{\nu}_a \nu_b), \quad (61)$$

where $C_{L,R} = \frac{g^2 e m_{a,b}}{32\pi^2 m_W^2} \times D_{L,R}$ and $\alpha_e \equiv e^2/(4\pi) \simeq 1/137$ in numerical investigations.

Because the charged Higgs boson have similar properties to those given in the 2HDM, we set a lower bound of $300 \text{ GeV} \leq m_\varphi \leq 2000 \text{ GeV}$, and $0.3 \leq t_\beta \leq 10$. Our investigation shows that the qualitative results of LFV decay do not change significantly, hence in the following illustration we fix $t_\beta = 3$ and $m_\varphi = 500 \text{ GeV}$. With different pairs of (ϕ, κ) given in Table II satisfying all experimental data of neutrino oscillation, the dependence of LFV decay $\text{Br}(\mu \rightarrow e \gamma)$ on the heavy RHN mass scale M_0 is shown in Fig. 20. We constrain the lower bound of exotic neutrino masses by $M_0 \geq \mathcal{O}(1) \text{ eV}$, leading to $|R| \sim \sqrt{\frac{m_0}{M_0}} \leq \mathcal{O}(10^{-1})$, so that the seesaw mechanism still works well.

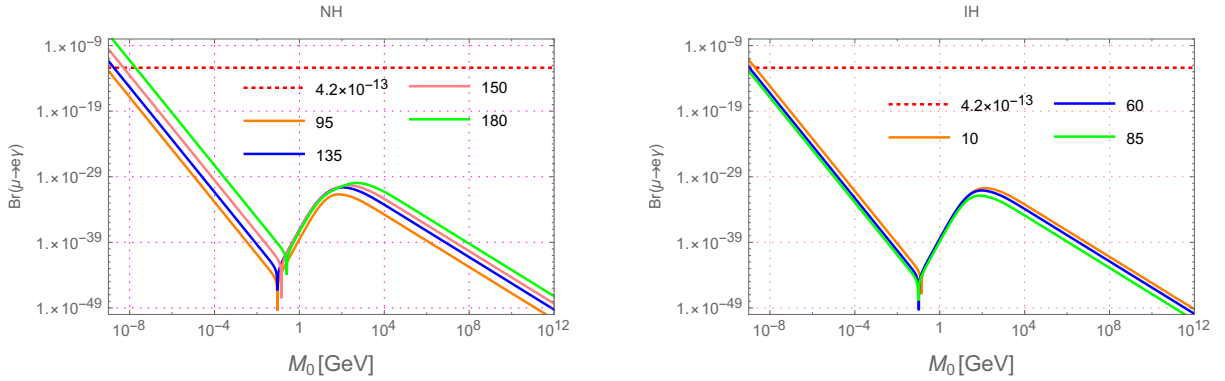


FIG. 20: $\text{Br}(\mu \rightarrow e \gamma)$ as a function of M_0 with different allowed values of (ϕ, κ) given in Table II and III for the NH and IH cases, where the values of $\phi = 95^\circ, 135^\circ, 150^\circ, 180^\circ$ or $10^\circ, 60^\circ, 85^\circ$ are pointed out in the respective figures. The red dotted lines show the experimental upper bound $\text{Br}(\mu \rightarrow e \gamma) < 4.2 \times 10^{-13}$.

The point to note is that $\text{Br}(\mu \rightarrow e \gamma)$ can approach the current experimental sensitivity $\text{Br}(\mu \rightarrow e \gamma) < 4.2 \times 10^{-13}$ [91] in the light exotic mass region, namely $M_{1,2,3} = \mathcal{O}(M_0) \sim$

$10^{-9} - 10^{-8}$ GeV. On the other hand, $\text{Br}(\mu \rightarrow e\gamma)$ is very suppressed with heavy M_i . Hence, if cLEV decays are detected, the region of heavy exotic neutrino masses is excluded, implying that leptogenesis and LFV data cannot be explained simultaneously in the model under consideration, i.e. the model is ruled out. We can see that the allowed region of $\text{Br}(\mu \rightarrow e\gamma) < 4.2 \times 10^{-13}$ results in very small values of $\text{Br}(\tau \rightarrow e\gamma)$ and $\text{Br}(\tau \rightarrow \mu\gamma)$; see an illustration in Figs. 21 and 22 for the HN and IH cases, respectively.

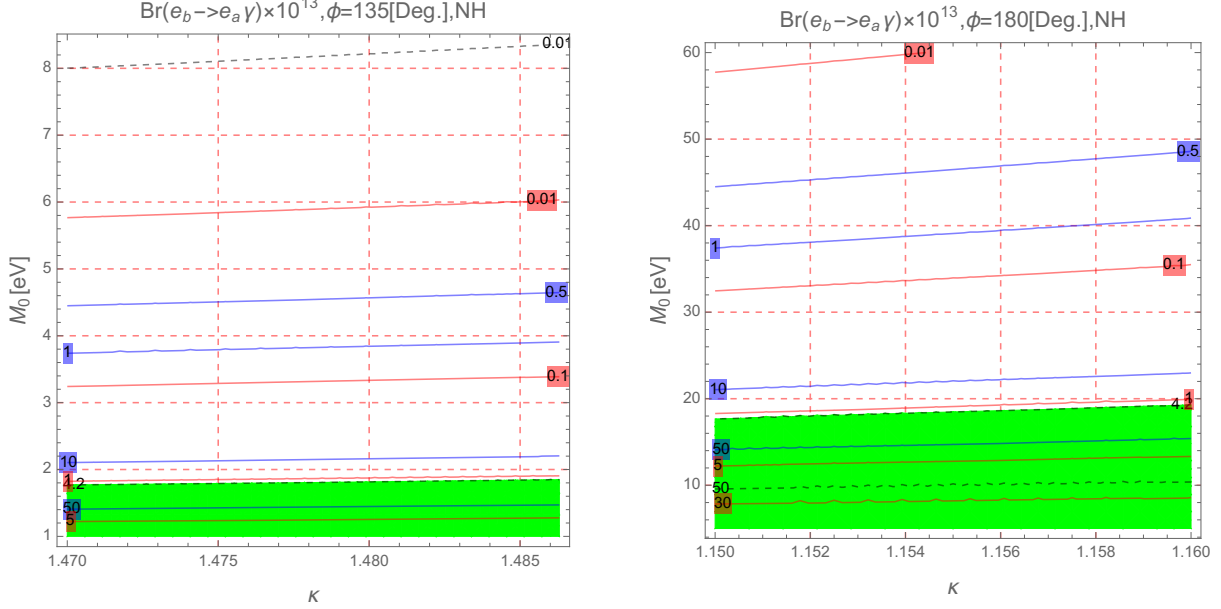


FIG. 21: Contour plots of $\text{Br}(e_b \rightarrow e_a \gamma)$ as functions of κ and M_0 in the NH case. The blue regions are excluded by $\text{Br}(\mu \rightarrow e\gamma) < 4.2 \times 10^{-13}$. The black dashed, red and blue curves show the constant values of $\text{Br}(\mu \rightarrow e\gamma)$, $\text{Br}(\tau \rightarrow e\gamma)$, and $\text{Br}(\tau \rightarrow \mu\gamma)$, respectively.

Generally, the constraint $\text{Br}(\mu \rightarrow e\gamma) < 4.2 \times 10^{-13}$ results in $\text{Br}(\tau \rightarrow \mu\gamma) \leq \mathcal{O}(10^{-12})$ and $\text{Br}(\tau \rightarrow e\gamma) \leq \mathcal{O}(10^{-13})$. These values are still much smaller than the sensitivity of near-future experiments [91–95]. In most allowed regions of parameters obtained from neutrino oscillation data, all of the values of $\text{Br}(e_b \rightarrow e_a \gamma)$ satisfy the experimental data of LFV decay, including in the region with heavy enough RHN masses to successfully explain the leptogenesis data.

In the above discussion, the neutrino mixing matrix defined in Eq. (54) is normally kept up to the order of $\mathcal{O}(R^2)$. The results may not be accurate for very light M_0 ; see the illustrations for the NH case shown in Fig. 23, where higher orders of R are included. Anyway, the $\text{Br}(\mu \rightarrow e\gamma)$, $\text{Br}(\tau \rightarrow e\gamma)$, and $\text{Br}(\tau \rightarrow \mu\gamma)$ are always well below the current experimental upper bounds. We note that our results predict that $\text{Br}(\mu \rightarrow e\gamma) < \mathcal{O}(10^{-29})$

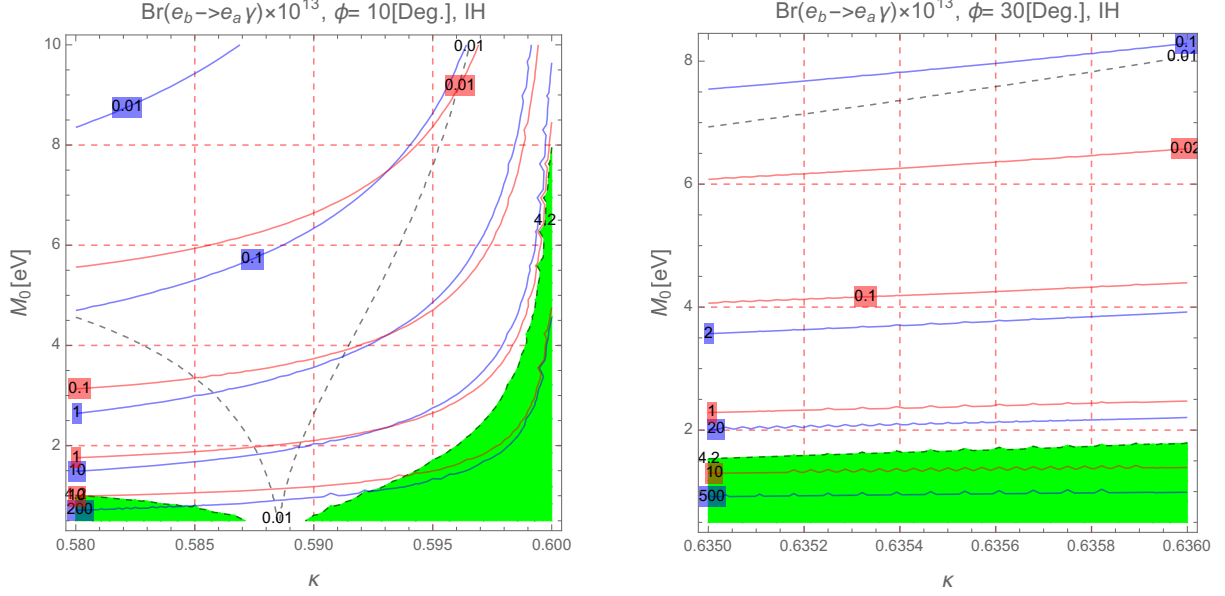


FIG. 22: Contour plots of $\text{Br}(e_b \rightarrow e_a \gamma)$ as functions of κ and M_0 in the NH case. The blue regions are excluded by $\text{Br}(\mu \rightarrow e \gamma) < 4.2 \times 10^{-13}$. The black dashed, red and blue curves show the constant values of $\text{Br}(\mu \rightarrow e \gamma)$, $\text{Br}(\tau \rightarrow e \gamma)$, and $\text{Br}(\tau \rightarrow \mu \gamma)$, respectively.

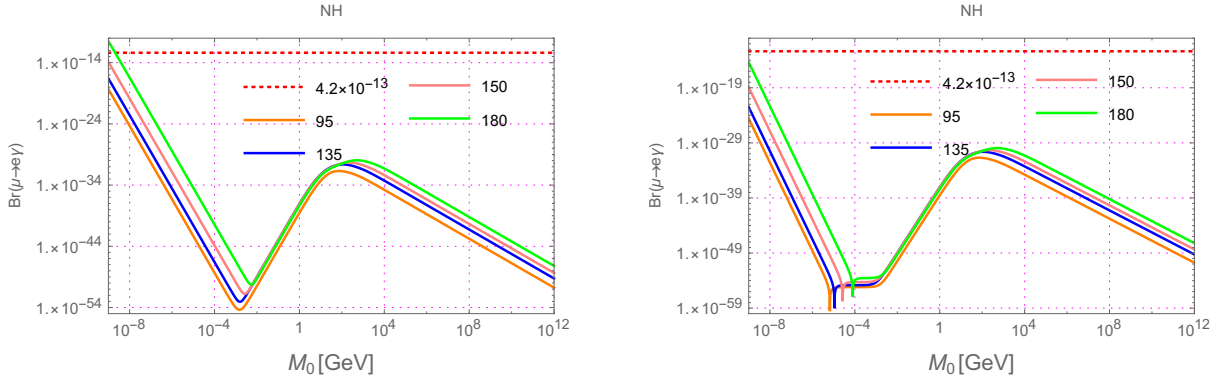


FIG. 23: Plots of $\text{Br}(e_b \rightarrow e_a \gamma)$ as functions of κ and M_0 in the NH case, where U^ν is kept up to $\mathcal{O}(R^4)$ and $\mathcal{O}(R^6)$ in the left and right panels, respectively.

with $1 \text{ GeV} < M_0 < 10^4 \text{ GeV}$. This is different from the results discussed in some previous work showing that the $\text{Br}(\mu \rightarrow e \gamma)$ can reach the current experimental bound [96]. The reason is that the Dirac matrix mass in Ref. [96] is defined following the Casas–Ibarra parameterization [97].

V. CONCLUSION

We have studied the seesaw version of an A_4 flavor symmetry model with two Higgs singlets beside other scalars as usual A_4 models. The allowed regions of the parameter space satisfying the current experimental neutrino oscillation data at 3σ CL are given numerically. We have found that the allowed ranges of κ and ϕ corresponding to the NH and the IH schemes separate completely. In particular, $\phi \in (90^\circ, 270^\circ)$ and $\kappa \in (1.15, 1.5)$ are allowed for the NH case, while $\phi \in (0^\circ, 90^\circ) \cup (270^\circ, 360^\circ)$ and $\kappa \in (0.55, 1)$ are allowed for the IH case. The model then predicts that the possible values of $|\langle m \rangle|$ will be $0.002 \text{ eV} \leq |\langle m \rangle| \leq 0.038 \text{ eV}$ for the NH and $0.048 \text{ eV} \leq |\langle m \rangle| \leq 0.058 \text{ eV}$ for the IH. This prediction is testable by running $0\nu 2\beta$ decay experiments, therefore is very clear information to confirm which NH or IH scheme is realistic. We have shown that the diagonal Hermitian matrix $H = Y_\nu Y_\nu^\dagger$ in the original model becomes non-diagonal after the effect of renormalization group evolution is included, therefore leptogenesis can be generated successfully in the allowed regions. The RHN mass scale $M_0 = 10^8 - 10^{12} \text{ GeV}$ is required for successful leptogenesis. In this range, it decreases with higher values of $\tan \beta$. Illustrations for η_B as functions of m_0 , ϕ , $|\langle m \rangle|$, and M_0 for different t_β have been presented. The minimum value of M_0 (10^8 GeV) corresponds to the so-called resonant leptogenesis where two heavy RHN masses M_1 and M_3 are almost degenerate (and also corresponds to the maximum value of $|\langle m \rangle|$ predicted by the model). We have found an interesting correlation between η_B and $|\langle m \rangle|$, so that once $|\langle m \rangle|$ is confirmed, we can pin down the RHN masses for successful leptogenesis for some given values of $\tan \beta$ as well as the absolute values of active neutrino masses.

We have also investigated the LFV decays of charged leptons, $e_a \rightarrow e_b \gamma$. Our investigation shows that if this signal is found experimentally in the future, the RHN mass scale must be smaller than the order of $\mathcal{O}(10 \text{ eV})$, so that the class of models we mentioned above must be improved to explain both LFV decays and leptogenesis, or they will be ruled out.

Acknowledgments

This research is funded by Vietnam National Foundation for Science and Technology Development (NAFOSTED) under grant number 103.01-2018.331.

Appendix A: A_4 group: the AF (Altarelli – Feruglio) basis introduced by G. Altarelli and F. Feruglio

The non-Abelian A_4 is a group of even permutations of four objects and has $4!/2 = 12$ elements. The group is generated by two generators S and T satisfying the relations

$$S^2 = (ST)^3 = (T^3) = 1. \quad (\text{A1})$$

There are three one-dimensional irreducible representations of the group denoted as

$$1 : \quad S = 1, \quad T = 1, \quad (\text{A2})$$

$$1' : \quad S = 1, \quad T = e^{i4\pi/3} \equiv \omega^2, \quad (\text{A3})$$

$$1'' : \quad S = 1, \quad T = e^{i2\pi/3} \equiv \omega. \quad (\text{A4})$$

It is easy to check that there is no two-dimensional irreducible representation of this group.

The three-dimensional unitary representations of T and S are given by

$$T = \begin{pmatrix} 1 & 0 & 0 \\ 0 & \omega^2 & 0 \\ 0 & 0 & \omega \end{pmatrix}, \quad S = \frac{1}{3} \begin{pmatrix} -1 & 2 & 2 \\ 2 & -1 & 2 \\ 2 & 2 & -1 \end{pmatrix}, \quad (\text{A5})$$

where T has been chosen to be diagonal. The multiplication rules for the singlet and triplet representations corresponding to the above basis of two generators T, S are given as

$$1 \times 1 = 1, \quad 1' \times 1'' = 1, \quad 3 \times 3 = 3 + 3_A + 1 + 1' + 1''. \quad (\text{A6})$$

For triplets

$$a = (a_1, a_2, a_3), \quad b = (b_1, b_2, b_3), \quad (\text{A7})$$

one can write

$$1 \equiv (ab) = (a_1 b_1 + a_2 b_3 + a_3 b_2), \quad (\text{A8})$$

$$1' \equiv (ab)' = (a_3 b_3 + a_1 b_2 + a_2 b_1), \quad (\text{A9})$$

$$1'' \equiv (ab)'' = (a_2 b_2 + a_1 b_3 + a_3 b_1). \quad (\text{A10})$$

Note that while 1 remains invariant under the exchange of the second and the third elements of a and b , $1'$ is symmetric under the exchange of the first and second elements while $1''$ is symmetric under the exchange of the first and third elements.

$$3 \equiv (ab)_S$$

$$= \frac{1}{3}(2a_1b_1 - a_2b_3 - a_3b_2, 2a_3b_3 - a_1b_2 - a_2b_1, 2a_2b_2 - a_1b_3 - a_3b_1), \quad (\text{A11})$$

$$3_A \equiv (ab)_A = \frac{1}{2}(a_2b_3 - a_3b_2, a_1b_2 - a_2b_1, a_3b_1 - a_1b_3). \quad (\text{A12})$$

We will only focus only on 3 since the 3_A terms are antisymmetric and hence cannot be used for the neutrino mass matrix. In the triplet 3, we can see that the first element has 2–3 exchange symmetry, the second element has 1–2 exchange symmetry, while the third element earns 1–3 interchange symmetry.

Moreover, if c, c', c'' are singlets of type $1, 1', 1''$, and $a = (a_1, a_2, a_3)$ is a triplet, then the products ac, ac', ac'' are triplets explicitly given by (a_1c, a_2c, a_3c) , (a_3c', a_1c', a_2c') , (a_2c'', a_3c'', a_1c'') , respectively.

Because the above basis, T is complex and $T^* \neq T$ in general, the complex conjugate representation r^* of a representation r ($r = 1', 1'', 3$) is not the same as r . It is determined by the following rules [98, 99]:

$$\begin{aligned} c \sim 1 \rightarrow c^* \sim 1, \quad c' \sim 1' \rightarrow c'^* \sim 1'^* = 1'', \quad c' \sim 1' \rightarrow c''^* \sim 1''^* = 1', \\ a = (a_1, a_2, a_3) \sim 3 \rightarrow a^* = (a_1^*, a_3^*, a_2^*). \end{aligned} \quad (\text{A13})$$

For the one-dimensional reps, it is easy to see these properties because $(\omega^2)^* = \omega$. For the 3-reps we can find a transformation U that changes 3^* into 3 or $3^* \sim 3$ and vice versa. This is similar to the case of $SU(2)$ symmetry. Namely, $UTU^{-1} = T^* = T^2$ and $USU^{-1} = S^* = S$ for T and S given in Eq. (A5). We can see this in the S_4 group where all of T, T^2 , and S are in the same conjugate class; see the details in Refs. [105, 106]. Hence, U belongs to S_4 but not A_4 , namely

$$U = TSTS^2 = \begin{pmatrix} 1 & 0 & 0 \\ 0 & 0 & 1 \\ 0 & 1 & 0 \end{pmatrix}. \quad (\text{A14})$$

In the model considered, the A_4 lepton triplet $\bar{\psi}^l = (\bar{\psi}_1^l, \bar{\psi}_2^l, \bar{\psi}_3^l) \sim 3$ has a complex conjugate of $\psi^l = (\psi_1^l, \psi_3^l, \psi_2^l) \sim 3^*$. The $3 \times 3^*$ is used for constructing the kinetic terms of lepton and Higgses, the Higgs potential, ... For example some quadratic terms respecting A_4 symmetry are:

$$\begin{aligned} \bar{\psi}^l &= (\bar{\psi}_1^l, \bar{\psi}_2^l, \bar{\psi}_3^l) \sim 3, \\ \rightarrow \quad \left(\bar{\psi}^l \gamma^\mu D_\mu \psi^l \right)_1 &= \bar{\psi}_1^l \gamma^\mu D_\mu \psi_1^l + \bar{\psi}_2^l \gamma^\mu D_\mu \psi_2^l + \bar{\psi}_3^l \gamma^\mu D_\mu \psi_3^l, \end{aligned}$$

$$\begin{aligned}
\phi_S &= (\phi_{S_1}, \phi_{S_2}, \phi_{S_3}) \sim 3, \quad \phi_S^* = (\phi_{S_1}^*, \phi_{S_3}^*, \phi_{S_2}^*) \sim 3^* \\
\rightarrow \quad &((D^\mu \phi_S)^\dagger D_\mu \phi_S)_1 = (D^\mu \phi_{S_1})^\dagger D_\mu \phi_{S_1} + (D^\mu \phi_{S_2})^\dagger D_\mu \phi_{S_2} + (D^\mu \phi_{S_3})^\dagger D_\mu \phi_{S_3}, \\
&((D^\mu \phi_T)^\dagger D_\mu \phi_T)_1 = (D^\mu \phi_{T_1})^\dagger D_\mu \phi_{T_1} + (D^\mu \phi_{T_2})^\dagger D_\mu \phi_{T_2} + (D^\mu \phi_{T_3})^\dagger D_\mu \phi_{T_3}, \\
\xi' \sim 1' \rightarrow \xi'^* \sim 1'^* = 1'' \rightarrow &(\xi'^* \xi')_1 = \xi'^* \xi', \quad (\xi''^* \xi'')_1 = \xi''^* \xi''. \tag{A15}
\end{aligned}$$

Note that the AF basis was used in Ref. [100].

Appendix B: Higgs potential and vacuum stability

Now we come to consider the Higgs potential which satisfies the condition of A_4 invariance,

$$\begin{aligned}
V_{H'} &= \mu_1^2 h_u^\dagger h_u + \mu_2^2 h_d^\dagger h_d + \mu_3^2 \xi'^\dagger \xi' + \mu_4^2 \xi''^\dagger \xi'' \\
&+ \lambda_1 (h_u^\dagger h_u)^2 + \lambda_2 (h_d^\dagger h_d)^2 + \lambda_3 (h_u^\dagger h_u)(h_d^\dagger h_d) \\
&+ \lambda_4 (h_u^\dagger h_d)(h_d^\dagger h_u) + \lambda^{\xi'} (\xi'^\dagger \xi')^2 + \lambda^{\xi''} (\xi''^\dagger \xi'')^2 + \lambda^{\xi' \xi''} (\xi'^* \xi')(\xi''^* \xi'') \\
&+ \lambda^{u \xi'} (h_u^\dagger h_u)(\xi'^* \xi') + \lambda^{d \xi'} (h_d^\dagger h_d)(\xi'^* \xi') + \lambda^{u \xi''} (h_u^\dagger h_u)(\xi''^* \xi'') \\
&+ \lambda^{d \xi''} (h_d^\dagger h_d)(\xi''^* \xi'') \\
&+ V(\phi_T) + V(\phi_S) + V(\phi_T, \phi_S) + V(\phi_T, h_u) + V(\phi_T, h_d) \\
&+ V(\phi_S, h_u) + V(\phi_S, h_d) + V(\phi_T, \xi', \xi'') + V(\phi_S, \xi', \xi''), \tag{B1}
\end{aligned}$$

where

$$\begin{aligned}
V(\phi_T) &= \mu_T^2 (\phi_T^\dagger \phi_T)_1 + \lambda_1^{\phi_T} (\phi_T^\dagger \phi_T)_1 (\phi_T^\dagger \phi_T)_1 + \lambda_2^{\phi_T} (\phi_T^\dagger \phi_T)_{1'} (\phi_T^\dagger \phi_T)_{1''} \\
&+ \lambda_3^{\phi_T} (\phi_T^\dagger \phi_T)_{3_A} (\phi_T^\dagger \phi_T)_{3_A} + \lambda_4^{\phi_T} (\phi_T^\dagger \phi_T)_{3_S} (\phi_T^\dagger \phi_T)_{3_S} \\
&+ \lambda_5^{\phi_T} (\phi_T^\dagger \phi_T)_{3_S} (\phi_T^\dagger \phi_T)_{3_A}, \\
V(\phi_S) &= \mu_S^2 (\phi_S^\dagger \phi_S)_1 + \lambda_1^{\phi_S} (\phi_S^\dagger \phi_S)_1 (\phi_S^\dagger \phi_S)_1 + \lambda_2^{\phi_S} (\phi_S^\dagger \phi_S)_{1'} (\phi_S^\dagger \phi_S)_{1''} \\
&+ \lambda_3^{\phi_S} (\phi_S^\dagger \phi_S)_{3_A} (\phi_S^\dagger \phi_S)_{3_A} + \lambda_4^{\phi_S} (\phi_S^\dagger \phi_S)_{3_S} (\phi_S^\dagger \phi_S)_{3_S} \\
&+ \lambda_5^{\phi_S} (\phi_S^\dagger \phi_S)_{3_S} (\phi_S^\dagger \phi_S)_{3_A}, \\
V(\phi_T, \phi_S) &= \lambda_1^{TS} (\phi_T^\dagger \phi_T)_1 (\phi_S^\dagger \phi_S)_1 + [\lambda_2^{TS} (\phi_T^\dagger \phi_T)_{1'} (\phi_S^\dagger \phi_S)_{1''} + \text{H.c.}] \\
&+ \lambda_3^{TS} (\phi_T^\dagger \phi_T)_{3_A} (\phi_S^\dagger \phi_S)_{3_A} + \lambda_4^{TS} (\phi_T^\dagger \phi_T)_{3_S} (\phi_S^\dagger \phi_S)_{3_S} \\
&+ \lambda_5^{TS} (\phi_T^\dagger \phi_S)_1 (\phi_S^\dagger \phi_T)_1 + \lambda_6^{TS} (\phi_T^\dagger \phi_S)_{1'} (\phi_S^\dagger \phi_T)_{1''} \\
&+ \lambda_7^{TS} (\phi_T^\dagger \phi_S)_{3_A} (\phi_S^\dagger \phi_T)_{3_A} + \lambda_8^{TS} (\phi_T^\dagger \phi_S)_{3_S} (\phi_S^\dagger \phi_T)_{3_S} \\
&+ [\lambda_9^{TS} (\phi_T^\dagger \phi_S)_{3_A} (\phi_S^\dagger \phi_T)_{3_S} + \text{H.c.}],
\end{aligned}$$

$$\begin{aligned}
V(\phi_T, h_u) &= \lambda^{Tu}(\phi_T^\dagger \phi_T)_1(h_u^\dagger h_u), \\
V(\phi_T, h_d) &= \lambda^{Td}(\phi_T^\dagger \phi_T)_1(h_d^\dagger h_d), \\
V(\phi_S, h_u) &= \lambda^{Su}(\phi_S^\dagger \phi_S)_1(h_u^\dagger h_u), \\
V(\phi_S, h_d) &= \lambda^{Sd}(\phi_S^\dagger \phi_S)_1(h_d^\dagger h_d), \\
V(\phi_T, \xi', \xi'') &= \lambda_1^{T\xi'\xi'}(\phi_T^\dagger \phi_T)_1(\xi'^* \xi') + \lambda_2^{T\xi''\xi''}(\phi_T^\dagger \phi_T)_1(\xi''^* \xi'') \\
&\quad + [\lambda_3^{T\xi'\xi''}(\phi_T^\dagger \phi_T)_{1''}(\xi'^* \xi'')_{1'} + \text{H.c.}], \\
V(\phi_S, \xi', \xi'') &= \lambda_1^{S\xi'\xi'}(\phi_S^\dagger \phi_S)_1(\xi'^* \xi') + \lambda_2^{S\xi''\xi''}(\phi_S^\dagger \phi_S)_1(\xi''^* \xi'') \\
&\quad + [\lambda_3^{S\xi'\xi''}(\phi_S^\dagger \phi_S)_{1''}(\xi'^* \xi'')_{1'} + \text{H.c.}].
\end{aligned} \tag{B2}$$

There are ten neutral Higgs components in the model, implying ten equations for the minimal condition of the Higgs potential in Eq. (B1). But only nine equations are independent of each other, namely

$$\begin{aligned}
\mu_1^2 + \lambda^{u\xi'} u'^2 + \lambda^{u\xi''} u''^2 + \lambda_3 v_d^2 + 3\lambda^{Su} v_S^2 + \lambda^{Tu} v_T^2 + 2\lambda_1 v_u^2 &= 0, \\
\mu_2^2 + \lambda^{d\xi'} u'^2 + \lambda^{d\xi''} u''^2 + 2\lambda_2 v_d^2 + 3\lambda^{Sd} v_S^2 + \lambda^{Td} v_T^2 + \lambda_3 v_u^2 &= 0, \\
\mu_3^2 u' + 2\lambda^{\xi'\xi'} u' u'^3 + \lambda^{\xi'\xi''} u' u''^2 + \lambda^{d\xi'} u' v_d^2 + 3\lambda_1^{S\xi'\xi'} u' v_S^2 + 3\lambda_3^{S\xi'\xi''} u'' v_S^2 \\
+ \lambda_1^{T\xi'\xi'} u' v_T^2 + \lambda^{u\xi'} u' v_u^2 &= 0, \\
\mu_4^2 u'' + 2\lambda^{\xi''\xi''} u'' u'^3 + \lambda^{\xi'\xi''} u'^2 u'' + \lambda^{d\xi''} u'' v_d^2 + 3\lambda_3^{S\xi'\xi''} u' v_S^2 + 3\lambda_2^{S\xi''\xi''} u'' v_S^2 \\
+ \lambda_2^{T\xi''\xi''} u'' v_T^2 + \lambda^{u\xi''} u'' v_u^2 &= 0, \\
\mu_T^2 + \lambda_1^{T\xi'\xi'} u'^2 + \lambda_2^{T\xi''\xi''} u''^2 + \lambda^{Td} v_d^2 + 3\lambda_1^{ST} v_S^2 + \lambda_5^{ST} v_S^2 \\
+ \lambda_6^{ST} v_S^2 + 2\lambda_7^{ST} v_S^2 + 6\lambda_8^{ST} v_S^2 + 2\lambda_1^T v_T^2 + 8\lambda_4^T v_T^2 + \lambda^{Tu} v_u^2 &= 0, \\
\lambda_3^{T\xi'\xi''} u' u'' + 3\lambda_2^{ST} v_S^2 + \lambda_5^{ST} v_S^2 + \lambda_6^{ST} v_S^2 - \lambda_7^{ST} v_S^2 - 3\lambda_8^{ST} v_S^2 &= 0, \\
\mu_S^2 + \lambda_1^{S\xi'\xi'} u'^2 + \lambda_3^{S\xi'\xi''} u' u'' + \lambda_2^{S\xi''\xi''} u''^2 + \lambda^{Sd} v_d^2 + 6\lambda_1^{ST} v_S^2 + 6\lambda_2^S v_S^2 \\
+ \lambda_1^{ST} v_T^2 + 4\lambda_4^{ST} v_T^2 + \lambda_5^{ST} v_T^2 + 4\lambda_8^{ST} v_T^2 + \lambda^{Su} v_u^2 &= 0, \\
\mu_S^2 + \lambda_1^{S\xi'\xi'} u'^2 + 2\lambda_3^{S\xi'\xi''} u' u'' + \lambda_2^{S\xi''\xi''} u''^2 + \lambda^{Sd} v_d^2 + 6\lambda_1^S v_S^2 + 6\lambda_2^S v_S^2 \\
+ \lambda_1^{ST} v_T^2 - 2\lambda_4^{ST} v_T^2 + \lambda_6^{ST} v_T^2 + \lambda_7^{ST} v_T^2 + \lambda_8^{ST} v_T^2 - 2\lambda_9^{ST} v_T^2 + \lambda^{Su} v_u^2 &= 0, \\
\mu_S^2 + \lambda_1^{S\xi'\xi'} u'^2 + 2\lambda_3^{S\xi'\xi''} u' u'' + \lambda_2^{S\xi''\xi''} u''^2 + \lambda^{Sd} v_d^2 + 6\lambda_1^S v_S^2 + 6\lambda_2^S v_S^2 \\
+ \lambda_1^{ST} v_T^2 - 2\lambda_4^{ST} v_T^2 + \lambda_7^{ST} v_T^2 + \lambda_8^{ST} v_T^2 + 2\lambda_9^{ST} v_T^2 + \lambda^{Su} v_u^2 &= 0.
\end{aligned}$$

These correspond to nine dependent parameters which are represented as functions of the remaining parameters in the Higgs potential, including the VEVs of neutral Higgs compo-

nents. The nine dependent parameters chosen in this work are $\mu_1^2, \mu_2^2, \mu_3^2, \mu_4^2, \mu_T^2, \mu_S^2, \lambda_4^{ST}, \lambda_6^{ST}$, and $\lambda_3^{T\xi'\xi''}$. Inserting them into Eq. (B1), the Higgs potential contains only independent parameters. The assumed vacuum alignments given in Table I satisfy the above minimal equations, hence this assumption can be dynamically achieved. Now, we can find the masses and mass eigenstates of Higgs bosons predicted by the model.

Regarding CP-odd neutral Higgs components, it is easily shown that the squared mass matrix has a zero determinant, which implies exactly a massless state corresponding to the Goldstone boson of the Z boson in the SM. On the other hand, this model must contain at least one SM-like Higgs bosons observed by the LHC. Hence, the squared mass matrix of the CP-even neutral Higgs bosons must contain this Higgs boson. The squared mass matrix of the CP-even Higgs components is a 10×10 matrix with a large number of Higgs self-couplings which are independent parameters. In this work we will choose a simple case of the Higgs potential that makes the Higgs spectrum realistic. In other words, the Higgs potential must satisfy the following conditions: (i) boundedness from below (BFB) and vacuum stability, (ii) all masses of physical Higgs are positive, (iii) having an SM-like Higgs boson observed by the LHC. Here we will focus mainly on the identification of an SM-like Higgs boson.

In general, the squared mass matrix of the CP-even Higgs bosons are a 10×10 matrix, where the main contribution to the SM-like Higgs boson arises from the two Higgs doublets h_u and h_d . Hence, we will choose the regime that these Higgs doublets decouple to other Higgs singlets, namely

$$\lambda^{u\xi'} = \lambda^{d\xi'} = \lambda^{u\xi''} = \lambda^{d\xi''}, \quad \lambda^{Tu} = \lambda^{Td} = \lambda^{Su} = \lambda^{Sd} = 0. \quad (\text{B3})$$

With this choice, the mass matrix will separate into two submatrices, a 2×2 and an 8×8 . The 8×8 matrix gives eight physical heavy Higgs bosons with masses depending on heavy VEVs v_S and v_T . In the original basis $(S_u, S_d)^T$, the 2×2 matrix contains an SM-like Higgs boson and has the form

$$M_1^2 = \begin{pmatrix} 4\lambda_1 v_u^2 & 2\lambda_3 v_u v_d \\ 2\lambda_3 v_u v_d & 4\lambda_2 v_d^2 \end{pmatrix}. \quad (\text{B4})$$

This gives two mass eigenstates, denoted as H_1 and H_2 . Their masses and relations with the original states are

$$m_{H_1}^2 = 2v^2 c_\beta^2 \left[\lambda_1 t_\beta^2 + \lambda_2 - \sqrt{(\lambda_1 t_\beta^2 - \lambda_2)^2 + \lambda_3^2 t_\beta^2} \right], \quad H_1 = S_u c_\alpha - S_d s_\alpha,$$

$$m_{H_2}^2 = 2v^2 c_\beta^2 \left[\lambda_1 t_\beta^2 + \lambda_2 + \sqrt{(\lambda_1 t_\beta^2 - \lambda_2)^2 + \lambda_3^2 t_\beta^2} \right], \quad H_2 = S_u s_\alpha + S_d c_\alpha, \quad (\text{B5})$$

where $s_\alpha \equiv \sin \alpha$, $c_\alpha \equiv \cos \alpha$, $s_{2\alpha} \equiv \sin 2\alpha$, and

$$\tan 2\alpha = \frac{\lambda_3 t_\beta}{\lambda_2 - \lambda_1 t_\beta^2}. \quad (\text{B6})$$

In the limit $\beta = \alpha + \pi/2$, we can show that the couplings of H_1 with other SM particles are the same as the SM predictions. Hence, in our model H_1 is identified with the SM-like Higgs boson found experimentally.

Regarding CP-odd neutral Higgs components, it is easily shown that the squared mass matrix has a zero determinant, which implies exactly a massless state corresponding to the Goldstone boson of the Z boson in the SM. Nine other CP-odd neutral Higgs are irrelevant to the phenomenology mentioned in this work.

Appendix C: Passarino–Veltman functions for LFV decays $e_b \rightarrow e_a \gamma$ ($b > a$)

The Passarino–Veltman functions, called C -functions, are defined as follows:

$$C_{0,\mu,\mu\nu}(M_1, M_2, M_2) \equiv \frac{1}{i\pi^2} \int \frac{d^4 k \times \{1, k_\mu, k_{\mu\nu}\}}{D_0 D_1 D_2}, \quad (\text{C1})$$

where $D_0 = k^2 - M_1^2$, $D_1 = (k + p_b)^2 - M_2^2$, and $D_2 = (k + p_a)^2 - M_2^2$, where $p_b \equiv p_1$ and $p_a \equiv p_2$ in usual notations for definitions of $C_{0,ij}$. The scalar C -functions are defined as $C_\mu = C_1 p_{b\mu} + C_2 p_{a\mu}$ and $C_{\mu\nu} = C_{00} g_{\mu\nu} + C_{11} p_{b\mu} p_{b\nu} + C_{12} (p_{b\mu} p_{a\nu} + p_{b\nu} p_{a\mu}) + C_{22} p_{a\mu} p_{a\nu}$. For LFV decay processes $e_b \rightarrow e_a \gamma$ we denote $p_{a,b}^2 = m_{a,b}^2$, where $m_{a,b}$ are the masses of the charged leptons $e_{a,b}$. The momentum of the photon $q = p_b - p_a$ satisfies $(p_b - p_a)^2 = q^2 = 0$. The C -functions in this case are,

$$\begin{aligned} C_0 &= \frac{t - 1 - t \ln t}{M_2^2 (t - 1)^2}, \quad C_1 = C_2 = -\frac{3t^2 - 4t + 1 - 2t^2 \ln t}{4(t - 1)^3 M_2^2}, \\ C_{11} &= C_{22} = 2C_{12} = \frac{11t^3 - 18t^2 + 9t - 2 - 6t^3 \ln t}{18M_2^2 (t - 1)^4}, \end{aligned} \quad (\text{C2})$$

where $t = M_1^2/M_2^2$. With $t = 1$, we have $C_0 = -1/(2M_2^2)$, $C_1 = 1/(6M_2^2)$ and $C_{11} = -1/(12M_2^2)$.

The definition of derivatives in Eq. (6) results in the definition of the tensor strength of gauge bosons as $F_{\mu\nu}^a = \partial_\mu W_\nu^a - \partial_\nu W_\mu^a + g\epsilon_{abc} W_\mu^b W_\nu^c$. The couplings of the photon to W^\pm

and ϕ^\pm are then determined as follows:

$$\begin{aligned} A_\mu \varphi^+ \varphi^- &: ie(p_+ - p_-)^\mu, \\ A_\lambda W_\mu^+ W_\nu^- &: -ie \left[g^{\lambda\mu} (q - p_+)^\nu + g^{\mu\nu} (p_+ - p_-)^\lambda + g^{\nu\lambda} (p_- - q)^\mu \right] \end{aligned} \quad (C3)$$

where q and p_\pm denote incoming photon momenta and $\varphi^\pm(W^\pm)$, respectively.

Contributions from W and φ^\pm bosons to $C_{L,R}$ are calculated based on the general form given in Ref. [101],

$$\begin{aligned} C_L^W &= -\frac{eg^2 m_a}{32\pi^2 m_W^2} \sum_{i=1}^6 U_{bi}^\nu U_{ai}^{\nu*} \left[2(C_{12} + C_{22} - C_1) m_W^2 + m_b^2 (C_{11} + C_{12} + C_1) \right. \\ &\quad \left. + m_{n_i}^2 (C_0 + C_1 + 2C_2 + C_{12} + C_{22}) \right], \\ C_R^W &= -\frac{eg^2 m_b}{32\pi^2 m_W^2} \sum_{i=1}^6 U_{bi}^\nu U_{ai}^{\nu*} \left[2(C_{11} + C_{12} - C_2) m_W^2 + m_a^2 (C_{12} + C_{22} + C_2) \right. \\ &\quad \left. + m_{n_i}^2 (C_0 + 2C_1 + C_2 + C_{11} + C_{12}) \right] \end{aligned} \quad (C4)$$

with $C_{0,a,ab} = C_{0,a,ab}(m_{n_i}, m_W, m_W)$, and

$$\begin{aligned} C_L^\varphi &= -\frac{m_a eg^2}{32\pi^2 m_W^2} \sum_{i=1}^6 U_{ai}^{\nu*} U_{bi}^L \times \left\{ t_\beta^2 m_b^2 (C_1 + C_{11} + C_{12}) \right. \\ &\quad \left. + m_{n_i}^2 [t_\beta^{-2} (C_2 + C_{12} + C_{22}) - (C_0 + C_1 + C_2)] \right\}, \\ C_R^\varphi &= -\frac{m_b eg^2}{32\pi^2 m_W^2} \sum_{i=1}^6 U_{ai}^{\nu*} U_{bi}^L \times \left\{ t_\beta^2 m_a^2 (C_2 + C_{12} + C_{22}) \right. \\ &\quad \left. + m_{n_i}^2 [t_\beta^{-2} (C_1 + C_{11} + C_{12}) - (C_0 + C_1 + C_2)] \right\} \end{aligned} \quad (C5)$$

with $C_{0,a,ab} = C_{0,a,ab}(m_{n_i}, m_\varphi, m_\varphi)$.

The formula for $C_{L,R}^W$ is consistent with that given in Refs. [96, 102–104] in the limit $m_a, m_b \ll m_W$ and $t_{W,i} \equiv \frac{m_{n_i}^2}{m_W^2}$, namely

$$\frac{C_L^W}{m_a} = \frac{C_R^W}{m_b} = -\frac{g^2 e}{32\pi^2 m_W^2} f_V(t_{Wi}), \quad f_V(t) = -\frac{10 - 43t + 78t^2 - 49t^3 + 4t^4 + 18t^3 \ln t}{12(t-1)^4} \quad (C6)$$

In the limit $m_{a,b} \rightarrow 0$ with $t_\beta = 1$ and $t_{\varphi,i} = \frac{m_{n_i}^2}{m_\varphi^2}$, the contributions from the charged Higgs bosons $C_{L,R}^\varphi$ have the following forms:

$$\frac{C_L^\varphi}{m_a} = \frac{C_R^\varphi}{m_b} = -\frac{g^2 e}{32\pi^2 m_W^2} f_s(t_{\varphi,i}), \quad f_s(t) \equiv \frac{t[7 - 12t - 3t^2 + 8t^3 - 6t(-2 + 3t) \ln t]}{12(t-1)^4}. \quad (C7)$$

-
- [1] P. F. Harrison, D. H. Perkins and W. G. Scott, Phys. Lett. B **530** (2002) 167 [hep-ph/0202074].
 - [2] P. F. Harrison and W. G. Scott, Phys. Lett. B **535**, 163 (2002) [hep-ph/0203209].
 - [3] P. F. Harrison and W. G. Scott, Phys. Lett. B **547** (2002) 219 [hep-ph/0210197].
 - [4] P. F. Harrison and W. G. Scott, Phys. Lett. B **557**, 76 (2003) [hep-ph/0302025].
 - [5] E. Ma and G. Rajasekaran, Phys. Rev. D **64**, 113012 (2001) [hep-ph/0106291].
 - [6] K. S. Babu, E. Ma and J. W. F. Valle, Phys. Lett. B **552** (2003) 207 [hep-ph/0206292].
 - [7] G. Altarelli and F. Feruglio, Nucl. Phys. B **720** (2005) 64 [hep-ph/0504165].
 - [8] G. Altarelli and F. Feruglio, Nucl. Phys. B **741** (2006) 215 [hep-ph/0512103].
 - [9] F. Bazzocchi, S. Kaneko and S. Morisi, JHEP **0803** (2008) 063 [arXiv:0707.3032 [hep-ph]].
 - [10] B. Brahmachari, S. Choubey and M. Mitra, Phys. Rev. D **77** (2008) 073008 Erratum: [Phys. Rev. D **77** (2008) 119901] [arXiv:0801.3554 [hep-ph]].
 - [11] B. Adhikary and A. Ghosal, Phys. Rev. D **78** (2008) 073007 [arXiv:0803.3582 [hep-ph]].
 - [12] F. Feruglio, C. Hagedorn, Y. Lin and L. Merlo, Nucl. Phys. B **775** (2007) 120 Erratum: [Nucl. Phys. B **836** (2010) 127] [hep-ph/0702194].
 - [13] M. C. Chen and K. T. Mahanthappa, Phys. Lett. B **652** (2007) 34 [arXiv:0705.0714 [hep-ph]].
 - [14] P. H. Frampton and T. W. Kephart, JHEP **0709** (2007) 110 doi:10.1088/1126-6708/2007/09/110 [arXiv:0706.1186 [hep-ph]].
 - [15] P. H. Frampton and S. Matsuzaki, Phys. Lett. B **679** (2009) 347 [arXiv:0902.1140 [hep-ph]].
 - [16] S. Pakvasa and H. Sugawara, Phys. Lett. **82B** (1979) 105.
 - [17] T. Brown, N. Deshpande, S. Pakvasa and H. Sugawara, Phys. Lett. **141B** (1984) 95.
 - [18] D. G. Lee and R. N. Mohapatra, Phys. Lett. B **329** (1994) 463 [hep-ph/9403201].
 - [19] E. Ma, Phys. Lett. B **632** (2006) 352 [hep-ph/0508231].
 - [20] M. Tanabashi *et al.* [Particle Data Group], Phys. Rev. D **98** (2018) no.3, 030001.
 - [21] G. Altarelli, F. Feruglio and L. Merlo, Fortsch. Phys. **61** (2013) 507 [arXiv:1205.5133 [hep-ph]].
 - [22] E. Ma, Phys. Rev. D **86** (2012) 117301 [arXiv:1209.3374 [hep-ph]].
 - [23] Y. H. Ahn, S. K. Kang and C. S. Kim, Phys. Rev. D **87** (2013) no.11, 113012 [arXiv:1304.0921 [hep-ph]].

- [24] M. C. Chen, J. Huang, J. M. O'Bryan, A. M. Wijangco and F. Yu, JHEP **1302** (2013) 021 [arXiv:1210.6982 [hep-ph]].
- [25] P. P. Novichkov, S. T. Petcov and M. Tanimoto, Phys. Lett. B **793** (2019) 247 [arXiv:1812.11289 [hep-ph]].
- [26] G. J. Ding, S. F. King and X. G. Liu, JHEP **1909** (2019) 074 [arXiv:1907.11714 [hep-ph]].
- [27] B. Karmakar and A. Sil, Phys. Rev. D **93** (2016) no.1, 013006 [arXiv:1509.07090 [hep-ph]].
- [28] S. Morisi, D. V. Forero, J. C. Romo and J. W. F. Valle, Phys. Rev. D **88** (2013) no.1, 016003 [arXiv:1305.6774 [hep-ph]].
- [29] B. Karmakar and A. Sil, Phys. Rev. D **91** (2015) 013004 [arXiv:1407.5826 [hep-ph]].
- [30] J. Barry and W. Rodejohann, Phys. Rev. D **81** (2010) 093002 Erratum: [Phys. Rev. D **81** (2010) 119901] [arXiv:1003.2385 [hep-ph]].
- [31] P. Minkowski, Phys. Lett. **67B** (1977) 421.
- [32] R. N. Mohapatra and G. Senjanovic, Phys. Rev. Lett. **44** (1980) 912.
- [33] M. Gell-Mann, P. Ramond and R. Slansky, Conf. Proc. C **790927** (1979) 315 [arXiv:1306.4669 [hep-th]].
- [34] T. Yanagida, Conf. Proc. C **7902131** (1979) 95.
- [35] J. Schechter and J. W. F. Valle, Phys. Rev. D **22** (1980) 2227.
- [36] M. Fukugita and T. Yanagida, Phys. Lett. B **174** (1986) 45.
- [37] G. F. Giudice, A. Notari, M. Raidal, A. Riotto and A. Strumia, Nucl. Phys. B **685** (2004) 89 [hep-ph/0310123].
- [38] W. Buchmuller, P. Di Bari and M. Plumacher, Annals Phys. **315** (2005) 305 [hep-ph/0401240].
- [39] S. M. Bilenky, S. Pascoli and S. T. Petcov, Phys. Rev. D **64** (2001) 053010 [hep-ph/0102265].
- [40] S. Pascoli, S. T. Petcov and L. Wolfenstein, Phys. Lett. B **524** (2002) 319 doi:10.1016/S0370-2693(01)01403-4 [hep-ph/0110287].
- [41] S. Pascoli, S. T. Petcov and W. Rodejohann, Phys. Lett. B **549** (2002) 177 [hep-ph/0209059].
- [42] S. T. Petcov, New J. Phys. **6** (2004) 109.
- [43] C. D. Froggatt and H. B. Nielsen, Nucl. Phys. B **147** (1979) 277. doi:10.1016/0550-3213(79)90316-X
- [44] G. Aad *et al.* [ATLAS Collaboration], Phys. Lett. B **716** (2012) 1 [arXiv:1207.7214 [hep-ex]].
- [45] S. Chatrchyan *et al.* [CMS Collaboration], Phys. Lett. B **716** (2012) 30 [arXiv:1207.7235

- [hep-ex]].
- [46] K. Asakura *et al.* [KamLAND-Zen Collaboration], AIP Conf. Proc. **1666** (2015) no.1, 170003 [arXiv:1409.0077 [physics.ins-det]].
 - [47] J. B. Albert *et al.* [EXO-200 Collaboration], Nature **510** (2014) 229 [arXiv:1402.6956 [nucl-ex]].
 - [48] A. Gando *et al.* [KamLAND-Zen Collaboration], Phys. Rev. Lett. **117** (2016) no.8, 082503 Addendum: [Phys. Rev. Lett. **117** (2016) no.10, 109903] [arXiv:1605.02889 [hep-ex]].
 - [49] W. Maneschg, “Present status of neutrinoless double beta decay searches,” arXiv:1704.08537 [physics.ins-det].
 - [50] A. Abada, . Hernndez-Cabezudo and X. Marcano, JHEP **1901** (2019) 041 [arXiv:1807.01331 [hep-ph]].
 - [51] M. Auger *et al.* [EXO-200 Collaboration], Phys. Rev. Lett. **109** (2012) 032505 [arXiv:1205.5608 [hep-ex]].
 - [52] O. Azzolini *et al.* [CUPID-0 Collaboration], Phys. Rev. Lett. **120** (2018) no.23, 232502 [arXiv:1802.07791 [nucl-ex]].
 - [53] D. Tosi [EXO-200 Collaboration], doi:10.1142/9789814603164_0047 arXiv:1402.1170 [nucl-ex].
 - [54] S. Obara [KamLAND-Zen Collaboration], Nucl. Instrum. Meth. A **845** (2017) 410.
 - [55] M. Agostini *et al.*, Nature **544** (2017) 47 [arXiv:1703.00570 [nucl-ex]].
 - [56] D. G. Phillips, II *et al.*, J. Phys. Conf. Ser. **381** (2012) 012044 [arXiv:1111.5578 [nucl-ex]].
 - [57] N. Abgrall *et al.* [LEGEND Collaboration], AIP Conf. Proc. **1894** (2017) no.1, 020027 [arXiv:1709.01980 [physics.ins-det]].
 - [58] D. R. Artusa *et al.* [CUORE Collaboration], Eur. Phys. J. C **74** (2014) no.8, 2956 [arXiv:1402.0922 [physics.ins-det]].
 - [59] D. R. Artusa *et al.* [CUORE Collaboration], Adv. High Energy Phys. **2015** (2015) 879871 [arXiv:1402.6072 [physics.ins-det]].
 - [60] J. Hartnell [SNO+ Collaboration], J. Phys. Conf. Ser. **375** (2012) 042015 [arXiv:1201.6169 [physics.ins-det]].
 - [61] A. S. Barabash, J. Phys. Conf. Ser. **375** (2012) 042012 [arXiv:1112.1784 [nucl-ex]].
 - [62] S. Karki, P. Aryal, H. J. Kim, Y. D. Kim and H. K. Park, Nucl. Instrum. Meth. A **877** (2018) 328.

- [63] J. J. Gomez-Cadenas *et al.* [NEXT Collaboration], Adv. High Energy Phys. **2014** (2014) 907067 [arXiv:1307.3914 [physics.ins-det]].
- [64] A. Abada, S. Davidson, A. Ibarra, F.-X. Josse-Michaux, M. Losada and A. Riotto, JHEP **0609** (2006) 010 [hep-ph/0605281].
- [65] S. Blanchet and P. Di Bari, JCAP **0703** (2007) 018 [hep-ph/0607330].
- [66] S. Antusch, S. F. King and A. Riotto, JCAP **0611** (2006) 011 [hep-ph/0609038].
- [67] S. Pascoli, S. T. Petcov and A. Riotto, Phys. Rev. D **75** (2007) 083511 [hep-ph/0609125].
- [68] S. Pascoli, S. T. Petcov and A. Riotto, Nucl. Phys. B **774** (2007) 1 [hep-ph/0611338].
- [69] G. C. Branco, R. Gonzalez Felipe and F. R. Joaquim, Phys. Lett. B **645** (2007) 432 [hep-ph/0609297].
- [70] G. C. Branco, A. J. Buras, S. Jager, S. Uhlig and A. Weiler, JHEP **0709** (2007) 004 [hep-ph/0609067].
- [71] J. A. Casas, J. R. Espinosa, A. Ibarra and I. Navarro, Nucl. Phys. B **556** (1999) 3 [hep-ph/9904395].
- [72] P. H. Chankowski and S. Pokorski, Int. J. Mod. Phys. A **17** (2002) 575 [hep-ph/0110249].
- [73] S. Antusch, J. Kersten, M. Lindner and M. Ratz, Phys. Lett. B **538** (2002) 87 [hep-ph/0203233].
- [74] G. C. Branco, R. Gonzalez Felipe, F. R. Joaquim and B. M. Nobre, Phys. Lett. B **633** (2006) 336 [hep-ph/0507092].
- [75] T. P. Nguyen and P. V. Dong, Adv. High Energy Phys. **2012** (2012) 254093.
- [76] Y. H. Ahn, C. S. Kim, S. K. Kang and J. Lee, Phys. Rev. D **75**, 013012 (2007) doi:10.1103/PhysRevD.75.013012 [hep-ph/0610007];
- [77] Y. H. Ahn and C. S. Chen, Phys. Rev. D **81** (2010) 105013 [arXiv:1001.2869 [hep-ph]].
- [78] Y. H. Ahn, S. K. Kang, C. S. Kim and T. P. Nguyen, Phys. Rev. D **82** (2010) 093005 [arXiv:1004.3469 [hep-ph]].
- [79] A. Pilaftsis and T. E. J. Underwood, Phys. Rev. D **72** (2005) 113001 [hep-ph/0506107].
- [80] N. Aghanim *et al.* [Planck Collaboration], Astron. Astrophys. **596** (2016) A107 [arXiv:1605.02985 [astro-ph.CO]].
- [81] V. Brdar, A. J. Helmboldt, S. Iwamoto and K. Schmitz, Phys. Rev. D **100** (2019) 075029 [arXiv:1905.12634 [hep-ph]].
- [82] I. Brivio, K. Moffat, S. Pascoli, S. T. Petcov and J. Turner, JHEP **1910** (2019) 059

- [arXiv:1905.12642 [hep-ph]].
- [83] J. A. Casas and A. Ibarra, Nucl. Phys. B **618** (2001) 171 [hep-ph/0103065].
 - [84] A. Ibarra, E. Molinaro and S. T. Petcov, JHEP **1009** (2010) 108 [arXiv:1007.2378 [hep-ph]].
 - [85] D. Gorbunov and I. Timiryasov, Phys. Lett. B **745** (2015) 29 [arXiv:1412.7751 [hep-ph]].
 - [86] G. C. Branco, P. M. Ferreira, L. Lavoura, M. N. Rebelo, M. Sher and J. P. Silva, Phys. Rept. **516** (2012) 1 [arXiv:1106.0034 [hep-ph]].
 - [87] H. T. Hung, T. T. Hong, H. H. Phuong, H. L. T. Mai and L. T. Hue, Phys. Rev. D **100** (2019) no.7, 075014 [arXiv:1907.06735 [hep-ph]].
 - [88] A. Vicente, Front. in Phys. **7** (2019) 174 [arXiv:1908.07759 [hep-ph]].
 - [89] N. H. Thao, L. T. Hue, H. T. Hung and N. T. Xuan, Nucl. Phys. B **921** (2017) 159 [arXiv:1703.00896 [hep-ph]].
 - [90] L. Lavoura, Eur. Phys. J. C **29** (2003) 191 [hep-ph/0302221].
 - [91] A. M. Baldini *et al.* [MEG Collaboration], Eur. Phys. J. C **76** (2016) no.8, 434 [arXiv:1605.05081 [hep-ex]].
 - [92] A. M. Baldini *et al.*, “MEG Upgrade Proposal,” arXiv:1301.7225 [physics.ins-det].
 - [93] A. Baldini *et al.* [Mu2e Collaboration], “Charged Lepton Flavour Violation using Intense Muon Beams at Future Facilities,” doi:10.2172/1568845
 - [94] B. Aubert *et al.* [BaBar Collaboration], Phys. Rev. Lett. **104** (2010) 021802 [arXiv:0908.2381 [hep-ex]].
 - [95] T. Aushev *et al.*, “Physics at Super B Factory,” arXiv:1002.5012 [hep-ex].
 - [96] A. Ibarra, E. Molinaro and S. T. Petcov, Phys. Rev. D **84** (2011) 013005 [arXiv:1103.6217 [hep-ph]].
 - [97] J. A. Casas and A. Ibarra, Nucl. Phys. B **618** (2001) 171 [hep-ph/0103065].
 - [98] F. Feruglio, C. Hagedorn, Y. Lin and L. Merlo, Nucl. Phys. B **809** (2009) 218 [arXiv:0807.3160 [hep-ph]].
 - [99] F. Feruglio, C. Hagedorn, Y. Lin and L. Merlo, Nucl. Phys. B **832** (2010) 251 [arXiv:0911.3874 [hep-ph]].
 - [100] S. F. King and C. Luhn, JHEP **1109** (2011) 042 [arXiv:1107.5332 [hep-ph]].
 - [101] L. T. Hue, L. D. Ninh, T. T. Thuc and N. T. T. Dat, Eur. Phys. J. C **78** (2018) no.2, 128 [arXiv:1708.09723 [hep-ph]].
 - [102] B. He, T. P. Cheng and L. F. Li, Phys. Lett. B **553** (2003) 277 [hep-ph/0209175].

- [103] D. N. Dinh, A. Ibarra, E. Molinaro and S. T. Petcov, JHEP **1208** (2012) 125 Erratum: [JHEP **1309** (2013) 023] [arXiv:1205.4671 [hep-ph]].
- [104] S. T. Petcov, Adv. High Energy Phys. **2013** (2013) 852987 [arXiv:1303.5819 [hep-ph]].
- [105] H. Ishimori, T. Kobayashi, H. Ohki, Y. Shimizu, H. Okada and M. Tanimoto, Prog. Theor. Phys. Suppl. **183** (2010) 1 [arXiv:1003.3552 [hep-th]].
- [106] F. Bazzocchi, L. Merlo and S. Morisi, Nucl. Phys. B **816** (2009) 204 [arXiv:0901.2086 [hep-ph]].